DEVELOPMENT OF A PULSE OXIMETER

A dissertation
submitted in partial fulfillment of the requirements
for the degree of

Master of Technology

by

Syrpailyne Wankhar

(Roll No. 03330003)

under the supervision of

Prof. P. C. Pandey

Biomedical Engineering Group
School of Biosciences and Bioengineering
Indian Institute of Technology, Bombay

July 2005

INDIAN INSTITUTE OF TECHNOLOGY, BOMBAY

M. Tech. Dissertation Approval

Dissertation entitled, "*Development of a Pulse Oximeter*", submitted by *Syrpailyne Wankhar (Roll No. 03330003)* is approved for the award of degree of *Master of Technology in Biomedical Engineering*.

Supervisor : _____ (Prof. P. C. Pandey)

Internal examiner : _____ (Prof. S. Mukherji)

External examiner : _____ (Prof. L. R. Subramanyan)

Chairman : _____ (Prof. T. S. Rathore)

Date: July 11, 2005

ACKNOWLEDGEMENTS

I would like to express my deepest gratitude to my guide Prof. P. C. Pandey for his precious guidance and support. His timely suggestions helped me to develop a better understanding of this project. I would like to thank Prof. S. Mukherji for the invaluable suggestions offered during the various stages of the project which enabled me to improve the work.

I am thankful to Mr. Dinesh S. Choudhary for rendering his valuable time and help in implementing the project. I also thank SPI lab mates, Mr. Vidyadhar Kamble, S. Navaneetha Krishnan Naidu, N. Narahari, B. Bhaskar Rao, Vinod K. Pandey, Dayashankar Dubey, and Sarika S. Gattawar for their cooperation.

Finally, my gratitude to my parents who have been a source of inspiration throughout my project work.

July 2005 **Syrpailyne Wankhar**

S. Wankhar / Prof. P. C. Pandey (supervisor): “Development of a Pulse Oximeter”, *M. Tech. dissertation*, Biomedical Engineering Group, School of Biosciences and Bioengineering, Indian Institute of Technology, Bombay, July 2005.

ABSTRACT

Pulse oximetry is a non-invasive technique that monitors the oxygen saturation of arterial blood. Light is passed through the tissue and the scattered light is collected with a photodiode positioned on an opposite surface (transmission mode) or an adjacent surface (reflectance mode). The light gets amplitude modulated by the pulsations of arterial blood caused by the cardiac activity, and the detected envelope is known as photoplethysmograms (PPG). Hemoglobin and oxyhemoglobin absorb light to varying degrees as a function of wavelength. Dual wavelength illumination (660 nm and 940 nm) of arterial blood, therefore, results in an absorption contrast that depends upon the proportion of hemoglobin that is chemically combined with oxygen. The circuit developed uses a reflectance mode sensor for high sensitivity, and a sensor circuit in which integration is used for noise rejection as well as auto ranging of sensor output for the two wavelengths. The instrument is to be used as part of cardiovascular diagnosis setup for simultaneous recording and analysis of ECG, phonocardiogram (PCG), impedance cardiogram (ICG), arterial pulse pressure, and oxygen saturation.

CONTENTS

Acknowledgements. **i**
Abstract **ii**
List of symbols **v**
List of abbreviations **vi**
List of figures **vii**
List of tables **ix**

Chapters
1. Introduction **1**
1.1 Overview 1
1.2 Project objective 1
1.3 Dissertation outline 2

2. Principle of pulse oximetry **3**
2.1 Introduction 3
2.2 Pulse oximetry technique 3
2.3 Photo diffusion based analysis 6
2.4 Beer Lambert based analysis 8
2.5 Pulse oximeters available 11
2.6 Instrument development 11

3. Hardware design of pulse oximeter **14**
3.1 Introduction 14
3.2 Signal Conditioning Unit 14
3.3 Control and Display Unit 23

4. Software description **27**
4.1 Introduction 27
4.2 Generation of square pulses 27
4.3 Signal acquisition 28

5. Validation of the hardware and test results **35**
5.1 Introduction 35
5.2 Voltage-to-current converter 35
5.3 Integrator 36
5.4 Low pass filter 37
5.5 Analog-to-digital converter 38
5.6 Test results 40

6. Summary and conclusion **44**
6.1 Summary of work done 44
6.2 Suggestions for future work 44

Appendix **45**
A Description of ADC functioning 45
B Power requirement 47
C Circuit diagram of pulse oximeter 48

References **51**

LIST OF SYMBOLS

Symbol	Explanation
I_t	Transmitted light intensity
I_o	Incident light intensity
V_a and V_v	Volume fractions of arterial and venous blood respectively
ε_a	Absorption coefficient
$\varepsilon_a^{tis}, \varepsilon_a^{ven}, \varepsilon_a$	Absorption coefficients of bloodless tissue layer, the venous blood layer, and the arterial blood layer, respectively
$\varepsilon'_{s,R}$	Transport corrected scattering coefficient in red spectral region
K_r	Function of the attenuation coefficient of the blood-perfused tissue, and the source to sensor path length
K_t	Function of the attenuation coefficient of the blood-perfused tissue and of the source to sensor path length.
r	The two wavelength (R/IR) ratio
$\sigma_a^{0\%}$	Optical absorption cross sections of the red blood cells containing totally deoxygenated hemoglobin (Hb)
$\sigma_a^{100\%}$	Optical absorption cross sections of the red blood cells containing totally oxygenated hemoglobin (HbO_2)
α , β, γ	Filter coefficients

LIST OF ABBREVIATIONS

Symbol	Explanation
SaO_2	Oxygen saturation
HbO_2	Oxygenated hemoglobin
Hb	Reduced hemoglobin
PPG	Photoplethysmogram
ICG	Impedance cardiogram
ECG	Electrocardiogram
RAP	Radial arterial pulse
ADC	Analog-to-digital converter
DC	Direct current
AC	Alternating current
BVP	Blood volume pulse
μC	Microcontroller
LED	Light emitting diode
S/H	Sample and Hold
R	Red
IR	Infrared
IIR	Infinite impulse response

LIST OF FIGURES

Fig. 2.1 Absorption coeff. vs wavelength for oxygenated and deoxygenated Hb [1]. 4

Fig. 2.2 Changes in sensor position leads to change in control volume [15]. 5

Fig. 2.3 Absorption of light by the arterial, venous, and pulsatile arterial components of blood [10]. 9

Fig. 2.4 Plot between the ratio *r* and the Oxygen Saturation based on Beer-Lambert model and other based on empirical data [1]. 10

Fig. 2.5 General block diagram of pulse oximeter. 12

Fig. 2.6 Reflectance pulse oximeter reflecting the optical sensor and the light sources [1]. 12

Fig. 3.1 Block diagram of pulse oximeter. 15

Fig. 3.2 Control pulses for the block diagram of Fig. 3.1. 16

Fig. 3.3 LED driver circuit with complementary control of R and IR sources. 18

Fig. 3.4 LED driver circuit with independent control of R and IR sources. 18

Fig. 3.5 Sensor circuit. 19

Fig. 3.6 Sample and hold circuit. 19

Fig. 3.7 Fourth order Butterworth low pass filter. 20

Fig. 3.8 Fourth order Butterworth LPF (DC separation) with AC/DC separator. 21

Fig. 3.9 Interface of 89C2051 microcontroller. 24

Fig. 3.10 Interface of the microcontroller ADuC812 to various circuits [17]. 26

Fig. 4.1 Timing and control pulses. 27

Fig. 4.2 Flowchart for calculation of SaO_2. 34

Fig. 5.1 Circuit for testing the integrator. 36

Fig. 5.2 Sensitivity of the integrator circuit. 37

Fig. 5.3 Magnitude response of the low pass filter. 37

Fig. 5.4 Plot between V_{in} and D_{out1} and D_{out2}. 39

Fig. 5.5 Control waveforms from the microcontroller port pins. 41

Fig. 5.6 Output waveform from the integrator. 42

Fig. 5.7 Output waveform from S/H circuit. 42

Fig. 5.8 AC+DC ir signal from fourth order Butterworth LPF. 42

Fig. 5.9 Output waveforms from AC/DC separator. 43

Fig. A.1	Internal ADC structure [17].	46
Fig. A.2	Buffering analog inputs.	46
Fig. C.1	Timing & control (TAC) ckt. : Power supply and the signal conditioning block.	48
Fig. C.2	Analog filter for red plethysmogram signal.	49
Fig. C.3	Analog filter for infrared plethysmogram signal.	50

LIST OF TABLES

Table 3.1	Functions of the various port pins of 89C2051 microcontroller.	23
Table 3.2	Functions of the various port pins of the ADuC812 microcontroller.	26
Table 4.1	Shows the count for the time duration given in Fig. 4.1.	28
Table 5.1	Performance of the V-I converter in Fig. 3.4.	35
Table 5.2	Test results for the integrator in Fig. 5.1.	32
Table 5.3	Frequency response of the filter.	36
Table 5.4	Test results for evaluation of linearity.	38
Table 5.5	Test results for evaluation of cross talk.	39
Table 5.6	Test results for the calculation of the AC/DC value.	40

Chapter 1
INTRODUCTION

1.1 Overview

Pulse oximetry non-invasively monitors the percentage of hemoglobin saturated with oxygen. Hemoglobin is the oxygen-carrying constituent of blood. Knowing what percentage of the hemoglobin is saturated with oxygen is important when providing anesthesia or for determining the effectiveness of the respiratory system as well as for diagnosing various illnesses. A pulse oximeter measures the absorption of red and infrared light passed through a patient's finger or ear lobe by utilizing light sensors. It depends on the difference between the absorption spectra between HbO_2 and Hb. Dual-wavelength measurements are usually made by placing two light emitting diodes whose spectral peaks are in the red and infrared regions and a photodiode on the same (or the opposite) side of the vascular bed. The photodiode senses the light that is reflected back from (or transmitted through) the tissues, which comprises of the alternating (AC) signal due to the absorption by pulsatile arterial blood superimposed on a steady-state (DC) level due to the attenuation caused by venous blood, skin pigments and other non-pulsatile components [1–4]. In most of the instruments, the DC level at each wavelength is used to normalize the corresponding AC signal amplitude. These AC components are used to calculate the absorption of oxyhemoglobin and deoxyhemoglobin. From this data the pulse oximeter does the mathematical calculations to determine the percentage oxygen saturation of the blood.

1.2 Project objective

This project is a continuation of earlier work done at IIT Bombay [5][6], and involves developing an instrument to acquire stable photoplethysmograms and further processing of this signal to display the arterial oxygen saturation. In addition to giving digital

readout, it should give the analog signals which can be digitized in parallel with the other physiologically related signals. The instrument may be used as part of cardiovascular diagnosis and research setup for simultaneous monitoring of ECG, phonocardiogram (PCG), impedance cardiogram (ICG), radial arterial pulse (RAP), photoplethysmogram (PPG) and oxygen saturation (SaO_2).

The main emphasis in the design is on developing a low cost compact versatile circuit for pulse oximeter, with all the control pulses generated by a microcontroller and flexibility for auto-ranging of internal waveforms.

The analog part of the instrument to acquire stable plethysmograms has been developed which is controlled using a microcontroller. The signals have been acquired digitally and processed to obtain arterial oxygen saturation which is displayed on LCD. This has been carried out by using a microcontroller with in-built analog-to-digital converter.

1.3 Dissertation outline

The second chapter describes the principle of pulse oximetry technique, Beer-Lambert and photon diffusion based analyses, and some commercially available instruments. The third chapter describes the two parts of the hardware: (i) signal conditioning unit consisting LED driver, integrator, sample and hold circuit, low pass filter circuit, AC/DC separator and (ii) control and display unit. Chapter 4 gives the software description. Chapter 5 describes the validation of the hardware and the test results. Chapter 6 summarizes the work done along with some suggestions for further work.

Chapter 2
PRINCIPLE OF PULSE OXIMETRY

2.1 Introduction

The pulse oximeter combines the technologies of spectrophotometry, which measures hemoglobin oxygen saturation, and optical plethysmography, which measures pulsatile changes in arterial blood volume at the sensor site [2]. Spectrophotometry uses various wavelengths of light to measure light absorption through given substances. Pulse oximeter passes red and infrared light into the sensor site and determines the absorption. Optical plethysmography uses light absorption technique to sense pulsatile blood volume. The changes that occur in the absorption of light due to change in the vascular bed produces a pulse that is time-varying and is known as the photoplethysmographic signal (PPG) or blood volume pulse (BVP). The pulse oximeter differentiates between optical absorption by blood and other anatomical constituents [1–4].

Inside the red blood cells, the oxygen chemically combines with hemoglobin (Hb) so that in the lungs it becomes saturated, forming a compound called oxyhemoglobin (HbO_2) and a very small amount of oxygen is dissolved in the plasma. The oxygen saturation (SaO_2) is the percentage concentration of oxyhemoglobin to the total hemoglobin concentration and is given by.

$$SaO_2 = 100\,[HbO_2] / ([HbO_2] + [Hb]) \qquad (2.1)$$

where,

$[HbO_2]$ = concentration of oxyhemoglobin.

[Hb] = concentration of reduced hemoglobin.

2.2 The pulse oximetry technique

Pulse oximetry is performed by placing the basic optical sensor consisting of two light

sources that emits red and infrared light into a pulsatile tissue (patient's finger or earlobe). The wavelength of the red LED is chosen from regions of the spectra where absorption coefficient of reduced hemoglobin is such that it absorbs about ten times as much light as oxyhemoglobin e.g., 660 nm. For the infrared LED the wavelength is chosen in the range of 940 nm, where the absorption coefficient of oxyhemoglobin is comparable with that of reduced hemoglobin [1–3][7–9]. At this wavelength the effect of oxygen level is almost constant. We can calculate the amount of oxygen by comparing the absorption outputs of each light source separately [10]. Fig. 2.1 shows the difference in absorption at these two wavelengths.

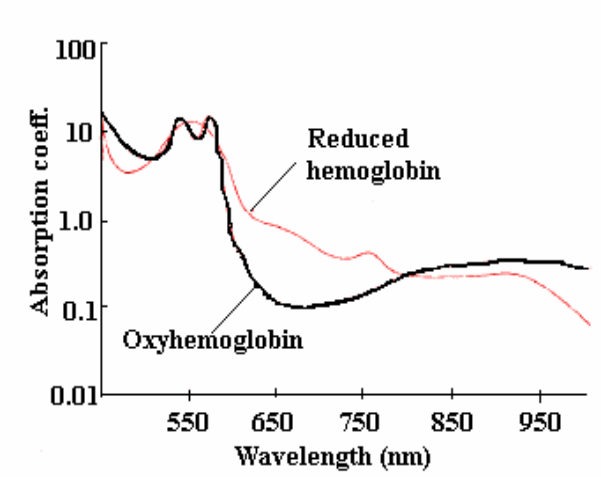

Fig. 2.1 Absorption coefficient versus wavelength for oxyhemoglobin and reduced hemoglobin [9].

Generally LED's are used to serve as light sources. The light from the two LEDs, is detected by a photodiode placed on an opposite surface (transmittance pulse oximetry) or on the adjacent surface (reflectance pulse oximetry). The light that is detected by the photodiode depends mainly on the opacity of the skin, reflection by the bones, tissue scattering and the amount of blood present in the vascular bed apart from the intensity of the incident light. The amount of light attenuated by the blood varies according to the pumping action of the heart. Consequently, as tissue blood volume increases during systole, the arterial blood absorbs a greater portion of the incident light causing rapidly alternating signal. Depending on the physiological state of the microvascular bed, alternating light intensity amounts to 0.05-1 % [4] of the total light intensity that is back scattered from (or transmitted through) the skin. Signals detected by the photodiode create photoplethysmogram (PPG) due to resulting cyclic light attenuation. The relative modulation of the red and infrared signals, which is known as red-infrared ratio is used to estimate the arterial oxygen saturation. Thus pulse oximetry is a pulse dependent technique, and any significant reduction in the amplitude of the pulsatile component of

the photoplethysmographic (PPG) signal detected by the oximeter can lead to inaccurate values for arterial oxygen saturation (SaO_2).

The accuracy of pulse oximeter tends to decrease due to motion artifacts, external lights, etc. Motion artifact is the major factor in the deterioration of accuracy; it results from a patient's respiration and/or movement. Motion of the sensor relative to the skin can cause an artifact that the pulse oximeter is unable to differentiate from normal arterial pulsations. Motion artifacts can usually be recognized by false or erratic pulse rate displays or distorted plethysmogram [2].

Pulse oximeter sensors employ either a reflectance or transmittance configuration. Fig. 2.2 shows the two modes of configuring the LED and photodetector, Fig. 2.2 (a) shows the reflectance sensor configuration and (b) shows the transmittance sensor configuration. Any changes in the position of the sensor will also lead to significant loss of the pulsatile signal because of the changes in the control volume monitored by the PPG signal [11]. The reflectance sensor configuration is more sensitive since the path through which the light travels is relatively small and consists of capillaries. A relatively large part of the light for the transmittance configuration consists of other tissue, not affected by pulsatile blood flow. But the reflectance sensor configuration is more affected by motion artifacts. This is because the absorption of light is mainly due to the capillaries that are extremely thin-walled vessels and collapse easily if any external pressures are applied. As the vessel walls collapse, the blood is pushed away from the region of increased pressure. Also any movement or compression caused to the tissue leads to redistribution of blood, which results in increased DC component and sometimes total loss of AC signal. The transmittance case has an advantage that the pulsatile changes in blood volume is mainly

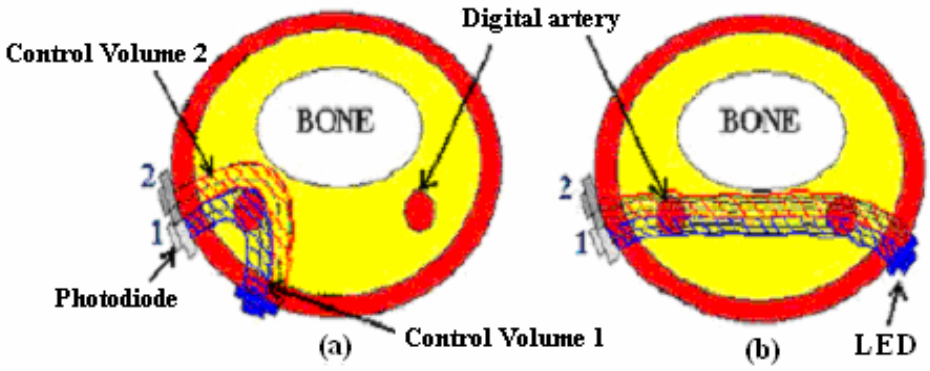

Fig. 2.2 Changes in sensor position leads to change in control volume [11].

due to the arteries and thus results in the strongest AC signal. In this configuration, large control volume is used as seen in Fig. 2.2 (b). Small changes in the distribution of blood have less effect on the overall PPG signal, and thus this configuration is less affected by motion artifacts [11].

2.3 Photon diffusion based analysis

Any change in the light intensity received by the detector is produced by the pulsatile flow of blood into and out of the tissue. The absorption coefficient of blood greatly exceeds that of the surrounding tissue, thus the influx arterial blood during systole increases the bulk absorption coefficient of the tissue, causing a transient reduction in the received intensity [12]. Thus for an increase in arterial blood volume ΔV_a, the total absorption is given as

$$\varepsilon_a + \Delta\varepsilon_a = \left(V_a + \Delta V_a\right)\varepsilon_a^{art} + V_v\varepsilon_a^{ven} + \left[1-\left(V_a + \Delta V_a + V_v\right)\right]\varepsilon_a^{tis}$$

so that,

$$\Delta\varepsilon_a = \Delta V_a\left(\varepsilon_a^{art} - \varepsilon_a^{tis}\right) \tag{2.2}$$

or,

$$\Delta\varepsilon_a \approx \Delta V_a\varepsilon_a^{art} \quad \text{for, } \varepsilon_a^{art} >> \varepsilon_a^{tis} \tag{2.3}$$

where,

V_a and V_v = volume fractions of arterial and venous blood respectively

ε_a^{tis} = absorption coefficient of the bloodless tissue

ε_a^{art} = absorption coefficient of the arterial blood

ε_a^{ven} = absorption coefficient of the venous blood

ε_a = absorption coefficient

Photon diffusion analysis assumes that the pulsatile component of the transmitted or reflected intensity measured by a pulse oximeter results from a change in absorption coefficient as described by Eqn. 2.3. Transient changes in the scattering coefficient and the venous component of the absorption coefficient are neglected [12]. The average

intensity I_r is known as the dc intensity, while ΔI_r is known as the ac intensity. The ac-dc ratio in case of reflection, according to photon diffusion analysis, is given by

$$\frac{\Delta I_r}{I_r} = \frac{3\varepsilon'_{s,R}}{2} K_r \varepsilon_a^{art} \Delta V_a \tag{2.4}$$

where,

K_r = function of the attenuation coefficient of the blood-perfused tissue, and the source to sensor path length.

$\varepsilon'_{s,R}$ = transport corrected scattering coefficient in red spectral region

For transmission case, the ac-dc ratio is given as

$$\frac{\Delta I_t}{I_t} = \frac{-3\varepsilon'_{s,R}}{2} K_t \varepsilon_a^{art} \Delta V_a \tag{2.5}$$

where,

K_t = function of the attenuation coefficient of the blood-perfused tissue and of the source to sensor path length.

The ac-dc ratio is obtained by measuring the pulsatile and average components of the sensor output. In the case of reflection, the ac-dc ratio at two wavelengths is given by

$$r \approx \frac{\left|\left(\Delta I_r / I_r\right)_R\right|}{\left|\left(\Delta I_r / I_r\right)_{IR}\right|} = \frac{\varepsilon'_{s,R} K_r}{\varepsilon'_{s,IR} K_r} \left(\frac{\varepsilon_{a,R}^{art}}{\varepsilon_{a,IR}^{art}}\right) \tag{2.6}$$

where,

$\varepsilon'_{s,IR}$ = transport corrected scattering coefficient in infrared spectral region.

The relationship of r and SaO_2, in the reflection case is given by

$$SaO_2 = \frac{r\sigma_{a,IR}^{0\%} - K'_r \sigma_{a,R}^{0\%}}{K'_r\left(\sigma_{a,R}^{100\%} - \sigma_{a,R}^{0\%}\right) + r\left(\sigma_{a,IR}^{0\%} - \sigma_{a,IR}^{100\%}\right)} \tag{2.7}$$

where, $K_r^{'} = \frac{\varepsilon_{s,R}^{'} K_r}{\varepsilon_{s,IR}^{'} K_r}$

In case of transmission, ac-dc ratio is given by

$$r \approx \frac{\left|\left(\Delta I_t / I_t\right)_R\right|}{\left|\left(\Delta I_t / I_t\right)_{IR}\right|} = \frac{\varepsilon_{s,R}^{'} K_t}{\varepsilon_{s,IR}^{'} K_t}\left(\frac{\varepsilon_{a,R}^{art}}{\varepsilon_{a,IR}^{art}}\right) \tag{2.8}$$

and the relationship of r and SaO_2, is given by

$$SaO_2 = \frac{r\sigma_{a,IR}^{0\%} - K_t^{'}\sigma_{a,R}^{0\%}}{K_t^{'}\left(\sigma_{a,R}^{100\%} - \sigma_{a,R}^{0\%}\right) + r\left(\sigma_{a,IR}^{0\%} - \sigma_{a,IR}^{100\%}\right)} \tag{2.9}$$

$$K_t^{'} = \frac{\varepsilon_{s,R}^{'} K_t}{\varepsilon_{s,IR}^{'} K_t}$$

where,

SaO_2 = fractional oxygen saturation of arterial blood

$\sigma_a^{100\%}$ and $\sigma_a^{0\%}$ = optical absorption cross sections of the red blood cells containing totally oxygenated (HbO_2) and totally deoxygenated hemoglobin (Hb) respectively

The quantity $K_t^{'}$ describes the effects of the dissimilar optical path lengths at the two wavelengths [12].

2.4 Beer-Lambert based analysis

In Photon diffusion analysis, the scattering effect is taken into account which is not the case in Beer-Lambert law analysis. Beer-Lambert law analysis is based on a compartmental model of tissue [12]. The tissue is modeled as consisting of three layers *i.e.*, bloodless tissue (thickness *T*), non-pulsatile venous and arterial blood (thickness *B*), and pulsatile arterial blood (thickness *A*). Fig. 2.3 demonstrates the static absorption components in the tissue along with one dynamic component *i.e.*, the pulse-added volume

of the arterial blood. Attenuation of the incident light by each layer is assumed to obey the Beer-Lambert law, so that the non-pulsatile transmitted intensity can be expressed as

$$I_t = I_o\left(e^{-\varepsilon_a^{tis}T}\right)\left(e^{-\varepsilon_a^{ven}B}\right)\left(e^{-\varepsilon_a A}\right) \tag{2.10}$$

where,

I_o = incident light intensity

$\varepsilon_a^{tis}, \varepsilon_a^{ven}, \varepsilon_a$ = absorption coefficients of bloodless tissue layer, the venous blood layer, and the arterial blood layer, respectively.

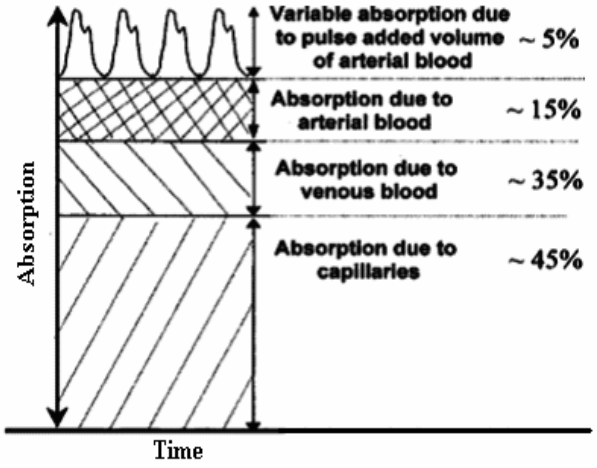

Fig. 2.3 Absorption of light by the arterial, venous, and pulsatile arterial components of blood [13].

It is assumed that small blood pulsations alter the thickness of the arterial blood layer which induces dynamics into the absorption characteristics of well-perfused peripheral sites. These dynamics are termed the photoplethysmographic signal (PPG). The total intensity can be differentiated with respect to A to obtain an expression for amplitude of the pulsatile ("AC") component of the transmitted intensity [4].

$$\frac{dI_t}{dA} = -I_o\left(e^{-\varepsilon_a^{tis}T}\right)\left(e^{-\varepsilon_a^{ven}B}\right)\left(e^{-\varepsilon_a A}\right) \tag{2.11}$$

The ac-dc ratio can be obtained by normalizing with respect to the non-pulsatile ("DC") intensity.

$$\frac{I_{ac}}{I_{dc}} = \frac{dI_t}{I_t} = -\varepsilon_a \, dA \tag{2.12}$$

The two wavelength ratio is used to calculate the level of oxygen by comparing the absorption outputs of the two light sources separately, it is given by

$$r = \frac{(dI_t/I_t)_R}{(dI_t/I_t)_{IR}} = \frac{\varepsilon_{a,R}^{art}}{\varepsilon_{a,IR}^{art}} \tag{2.13}$$

R and IR correspond to values at a specific wavelength in the red or near-infrared spectral region. The relationship between r and SaO_2 that results from the Beer-Lambert analysis is given as

$$SaO_2 = \frac{r\sigma_{a,IR}^{0\%} - \sigma_{a,R}^{0\%}}{\left(\sigma_{a,R}^{100\%} - \sigma_{a,R}^{0\%}\right) + r\left(\sigma_{a,IR}^{0\%} - \sigma_{a,IR}^{100\%}\right)} \tag{2.14}$$

The Beer-Lambert model is applicable for the transmission case in which the optical path length at the two wavelengths is constant, independent of the optical properties of the tissue. Fig. 2.4 shows two relationships, one using the Beer-Lambert law and the other based on empirical data, between the ratio r and the oxygen saturation (SaO_2). Consequently, instruments based on the Beer-Lambert law tended to give erroneous estimates of the true value of oxygen saturation (especially for SaO_2 values below 85%) [3].

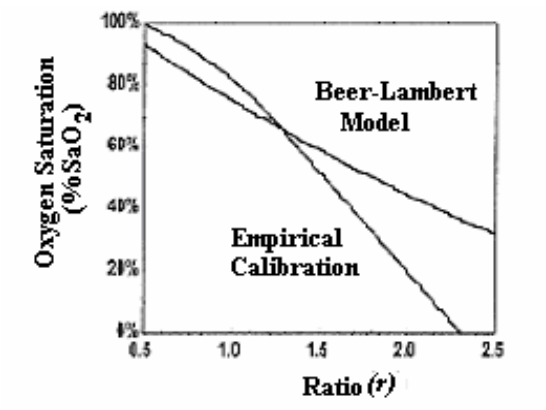

Fig. 2.4 Plot between the ratio r and the oxygen saturation based on Beer-Lambert model and other based on empirical data [3].

2.5 Pulse oximeters available

Pulse oximeter is completely noninvasive and gives continuous real-time estimates of arterial oxygen saturation. It was first developed by Matthes in 1935 [14]. In 1988, Association of Anaesthetists of Great Britain & Ireland (AAGB&I), recognized it as their standard for intraoperative monitoring [14]. In 1990, it became an American Society of Anesthesiologists (ASA) standard for intraoperative monitoring [14]. Some of the commercially available instruments are listed below:

(i) Pulse oximeter "NPB-290", from Nellcor, Pleasanton, CA, USA. The design has a US patent [15].

(ii) Pulse oximeter "504DX", from Criticare Systems, Inc., Waukesha, WI, USA [16].

(iii) "3303" Hand-Held Pulse oximeter, from Smiths Medical PM, Inc., Waukesha, WI, USA. The design has a US patent [17].

(iv) Pulse oximeter "3800/P", from G.E Healthcare, Chalfont St. Giles, UK [18].

(v) Pulse oximeter "Rad-9", from Masimo, Irvine, CA, USA. This design has a US patent [19].

2.6 Instrument development

General block diagram of pulse oximeter is given in Fig. 2.5. It consists of the finger tip probe, excitation source, timing and pulse generator, current-to-voltage (I-V) converter, sample and hold (S/H) circuit, filters, analog-to-digital converter (ADC), computation and display unit. The excitation source may be a voltage source with a current limiting resistor [10] or a current source [1][7][11]. The finger tip probe contains the red (R) and infrared (IR) LED's as light sources and a photodetector (S) that is placed either in transmittance or reflection configuration. Fig. 2.6 shows the placement of the LED's and photodetector in reflectance configuration. The peak wavelength of the red LED is 660 nm, and that of the infrared LED is 940 nm [1–3][7][10]. The excitation source drives the R and IR LED's with control from timing and pulse generator and the photodetector senses the light emitted by the two light sources. Microprocessors [4][11][15][20] or discrete components [7] are used for generating the timing and control pulses for various parts of the circuits. The photodetector output is a current and is given to the I-V converter for processing. The signal is demultiplexed with S/H and the output consists of

both AC and DC components with respect to red and infrared LED. Filtering for AC/DC separation is done. The four analog signals (R-ac, R-dc, IR-ac, IR-dc) are digitized using an ADC. The digitized values are fed to the microcontrollers or microprocessors [4][10][15], which calculate the oxygen saturation by determining how much of each type of light was absorbed by the hemoglobin and computing the ratio of red and infrared light absorbed. The value of oxygen saturation is displayed using a PC [6][7] or a LCD display [14][15].

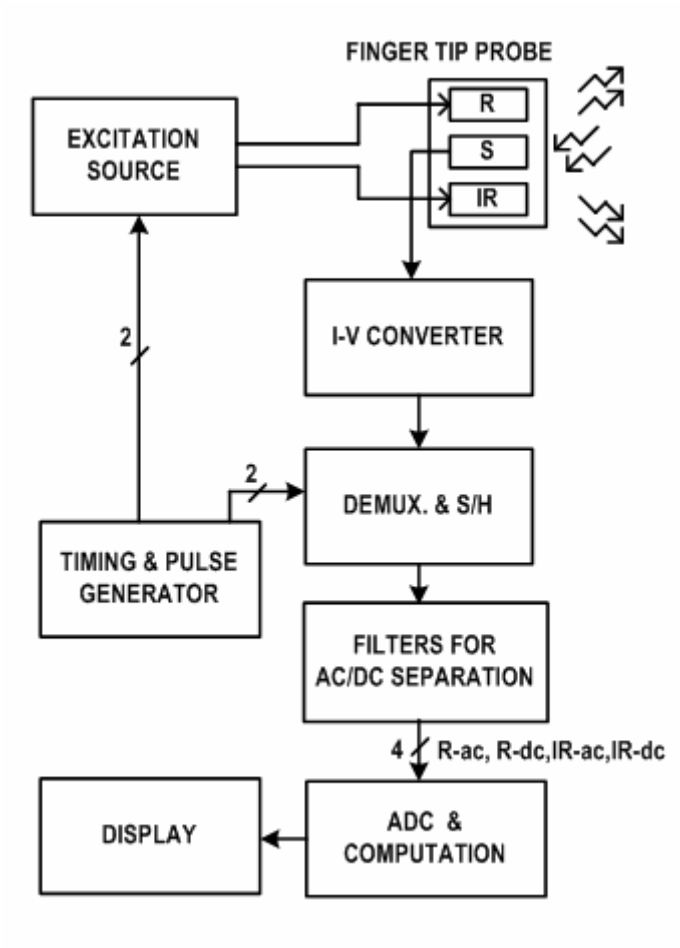

Fig. 2.5 General block diagram of pulse oximeter.

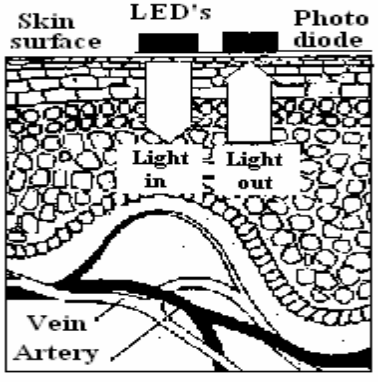

Fig. 2.6 Reflectance pulse oximeter reflecting the optical sensor and the light sources [1].

S. S. Adsul [5] and M. Ingle [6], as part of their dissertations at IIT Bombay, worked towards developing the pulse oximeter with design approach discussed above. The same approach has been used in this project, with certain modifications to overcome existing shortcomings. Based on the discussion in section 2.3 and 2.4 on the two models of pulse oximetry analysis it has been decided to use Eqn. 2.7 based on photon diffusion analysis, for estimation of oxygen saturation in arterial blood. The following chapter provides a description of the complete hardware.

Chapter 3
HARDWARE DESIGN OF PULSE OXIMETER

3.1 Introduction

The block diagram of the hardware of the pulse oximeter is given in Fig. 3.1. The hardware can be divided into two parts: (i) signal conditioning unit and (ii) control and display unit. The control and display unit has two microcontrollers at its core. The timing and control unit generates all timing and control signals for the signal conditioning unit, and the acquisition, processing and display unit acquires the signals through analog-to-digital converter, and calculates the R/IR ratio which is used in the calculation of oxygen saturation and the results are displayed on a LCD display.

The sensor assembly consists of red and infrared LED's as light sources and a photodiode as a photo sensor. The two LED's are connected in anti-parallel and are turned on by current flow in opposite directions. This arrangement saves a wire. The output signal from the photodiode is processed by signal conditioning circuit, which gives two photoplethysmographic signals, and these signals are then separated into AC and DC part. Four analog signals V_{acR}, V_{acIR}, V_{dcR}, and V_{dcIR} are digitized using analog-to-digital converter. The microcontroller takes these digital values and calculates the R/IR ratio and then determines the SaO_2. SaO_2 obtained and pulse rate are displayed on a LCD display.

This chapter gives a brief description of each block of the overall hardware of Fig. 3.1. The last section describes the interfacing of the microcontroller to these blocks.

3.2 Signal conditioning unit

In the signal conditioning unit, an infrared LED and red LED are alternately driven using output from one of the port pins of the microcontroller and voltage-to-current converter. The light, which is reflected back, is sensed by a single photodiode. The photodiode converts the light into proportional current. To reduce high frequency noise, the current is

converted to voltage using an integrator. The signal from the integrator is sampled by using two sample-and-hold circuits (S/H) to give the signal corresponding to red and infrared pulses separately. Another feature of the circuit is that the integration time before S/H can be used to control the voltage gain for the red and infrared outputs independently. The current pulses for driving the red and infrared LED's are controlled by two of the microcontroller port pins and are well separated. The control signals for S/H circuits are also generated by the microcontroller. For the S/H-R, the control signal is generated before V_1 goes low. Similarly control signal to S/H-IR is generated after V_2 goes high. After each sampling of the integrated output, control V_5 to an analog switch discharges the capacitor of the integrator. Each S/H output is fed to a low pass filter for smoothening the signal. This output contains both AC and DC components. For separating the DC signal another low pass filter is used. This signal is then subtracted from the composite signal to obtain the AC signal. The control voltages in Fig. 3.1 are shown in Fig. 3.2

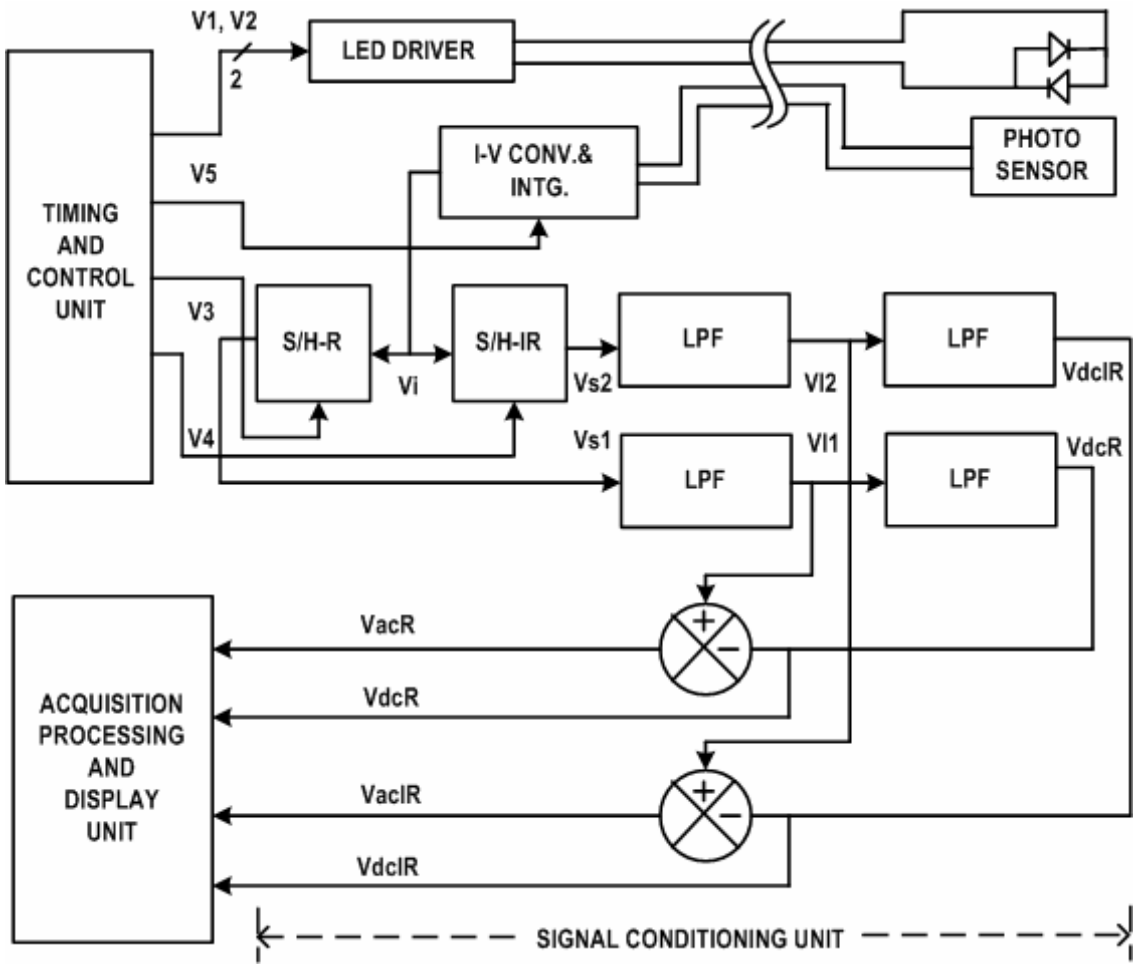

Fig. 3.1 Block diagram of pulse oximeter.

The integrator is reset before transmission of light pulses. The integrator output is read by the S/H circuit at a duration which is selected for appropriate scaling of the output. A finite gap is left between the red and infrared pulses as shown in Fig. 3.2.

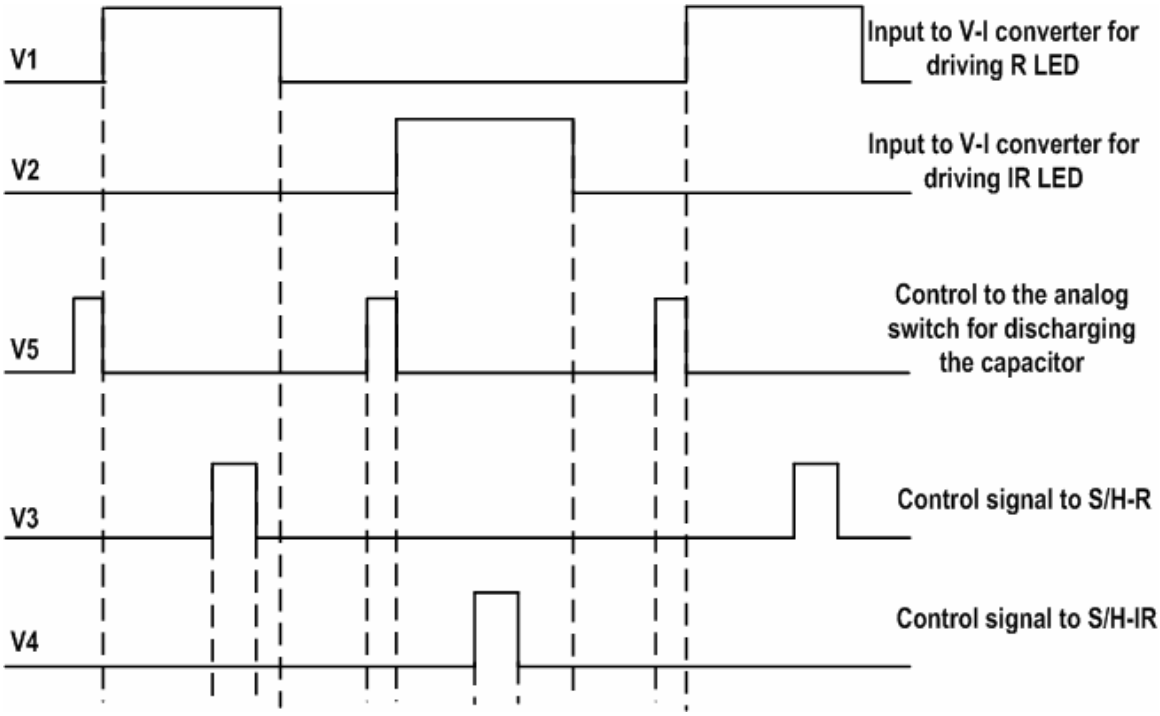

Fig. 3.2 Control pulses for block diagram of Fig. 3.1.

3.2.1 LED driver

The red and infrared LED's, used as light sources are connected in anti-parallel. This arrangement reduces the number of wires to the sensor assembly. Either one of the LED's can be turned on depending on the current direction.

Our first design of the LED driver, shown in Fig. 3.3, consisted of a comparator and V-I converter. The square pulse V_1, generated from the microcontroller, is given to the comparator, the bipolar V-I converter drives the two LEDs alternately. The disadvantage in this case is that there is no clear gap between the light from the two sources, and this introduces a cross-talk between the two channels. For Fig. 3.3, the LED drive current is given by

$$I = \frac{1}{R_6}\left(\frac{R_5}{R_4 + R_5} V_X\right) \tag{3.1}$$

with V_x = 5V; R_6 = 80 Ω

$$I_r = \frac{1}{80}\left(\frac{330}{330+330}\times 5\right) = 31.25\,\text{mA}$$

(I_{ir} = 31.25 mA, with $V_x = -5$ V).

The circuit was modified to provide independent control of the two LED's, as shown in Fig. 3.4. Two square waves of approximately 300 Hz are generated from the port pins of the microcontroller. A bipolar V-I converter drives the two LEDs using these square waves, permitting independent turning on of the two LEDs. In the circuit diagram of Fig. 3.4, let $\alpha' = R_8/R_6$ and $\beta' = R_9/R_4$. For virtual short at the inputs of op amp IC2A, we have

$$V_1'\frac{\alpha'}{1+\alpha'} + V_4\frac{1}{1+\alpha'} = V_2'\frac{\beta'}{1+\beta'} + V_3\frac{1}{1+\beta'}$$

On rearranging this gives

$$V_4 = \frac{\alpha'+1}{\beta'+1}V_3 + \frac{\alpha'+1}{\beta'+1}\beta' V_2' - \alpha' V_1' \qquad (3.2)$$

By selecting $\alpha' = \beta'$, we get

$$V_3 - V_4 = \alpha'(V_1' - V_2') \qquad (3.3)$$

From Eqn. 3.3, when V_1' is high, I_r will be the current flowing in the direction as shown in Fig. 3.4 and the red LED will be turn on and similarly when V_2' is high, I_{ir} will be the current flowing and infrared LED will be turn on. With the component values selected, α' = 1 and with V_1' = 2.3 V; V_2' = 1.0 V and R_{11} = 68 Ω, the LED drive current for Fig. 3.4 is given by

$$I = \alpha'\frac{V_3 - V_4}{R_{11}} = \alpha'\frac{V_1' - V_2'}{R_{11}} \qquad (3.4)$$

with $V_1' = 2.3\text{V}$; $V_2' = 0\text{V}$,

$$I_r = \left(\frac{2.3-0}{68}\right) = 33.8 \text{ mA}$$

and with $V_1' = 0$ V; $V_2' = 1.0\text{V}$, $I_{ir} = \left(\frac{0-1.0}{68}\right) = 14.7$ mA.

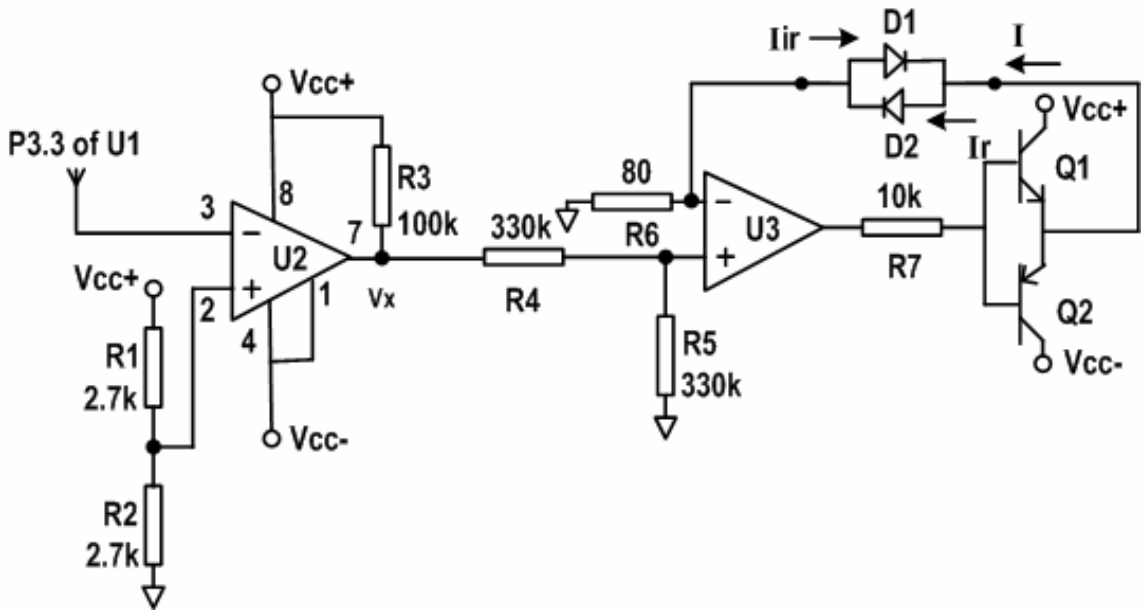

Fig. 3.3 LED driver circuit with complementary control of R and IR sources.
(U1: AT89C2051, U2: LM 311, U3: TL084, Q1: SL100, Q2: SK100).

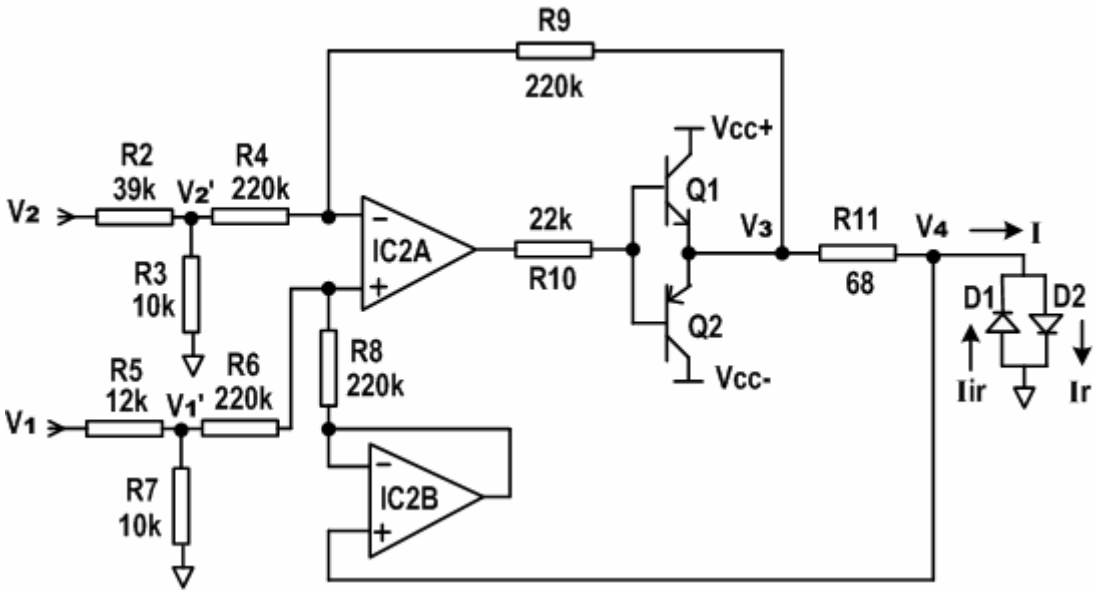

Fig. 3.4 LED driver circuit with independent control of R and IR sources.
(IC2A, IC2B: TL084, Q1: SL100, Q2: SK100).

3.2.2 Sensor circuit

For detection of light, a photodiode can be used in two modes, one is active mode or photovoltaic mode and other is passive mode or photoconductive mode [21]. No external biasing is required in photovoltaic mode. In this case noise problem is less as compared to photoconductive mode, but it has a disadvantage of slow response and low sensitivity. Photoconductive mode requires external biasing; it has high speed of response and better sensitivity. The output of the photodiode is a current and it has higher sensitivity to infrared as compared to red light. For processing, this signal current should be converted to voltage. We use an integrator as shown in Fig. 3.5, for noise reduction.

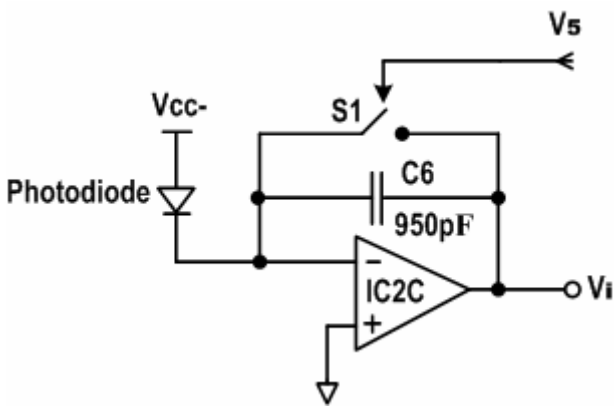

Fig.3.5 Sensor circuit
(IC2C: TL084).

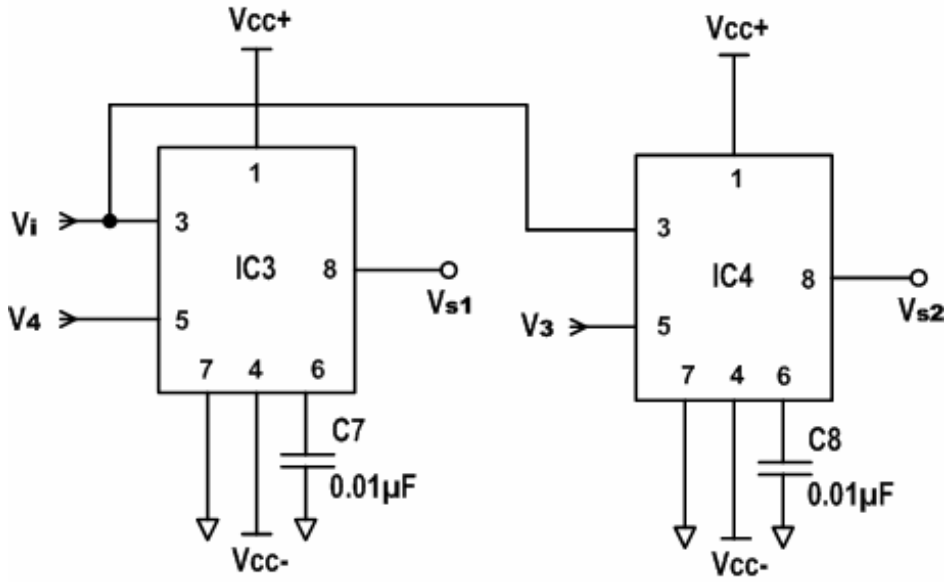

Fig. 3.6 Sample and hold circuit
(IC3, IC4: LF 398).

The op-amp used in the integrator should have very low bias current because photodiode current should not get swamped by bias current of op-amp. Hence JFET input op-amp TL084 is used. We get ramp signal at the integrator output. IC-CD4066 is used as a switch for discharging the capacitor before application of the next light pulse. Sensitivity of the output voltage can be controlled, to a certain extent, by the integration duration.

3.2.3 Sample-and-Hold circuit

The output from the integrator is sampled and held by two S/H circuits. This stage separates the two signals resulting from the activation of the two LED's. Control signal to S/H-R is driven by the pulse that is being generated by the microcontroller before V_1 goes low and the same is done for the other S/H-IR before the V_2 goes high. The S/H circuit is build using IC-LF398. The circuit diagram is as shown in Fig 3.6.

3.2.4 Low pass filter

The output of the sample and hold circuits are step-like signals and are noisy. The dominant noise is 100 Hz pickup due to ambient light. To get smooth and noise free signals, the S/H outputs are fed to fourth order low pass Butterworth filter as shown in Fig. 3.7. We choose a cut off frequency of 10 Hz since plethysmographic signal has information mainly below 10 Hz; the gain of this filter is kept at 2.53.

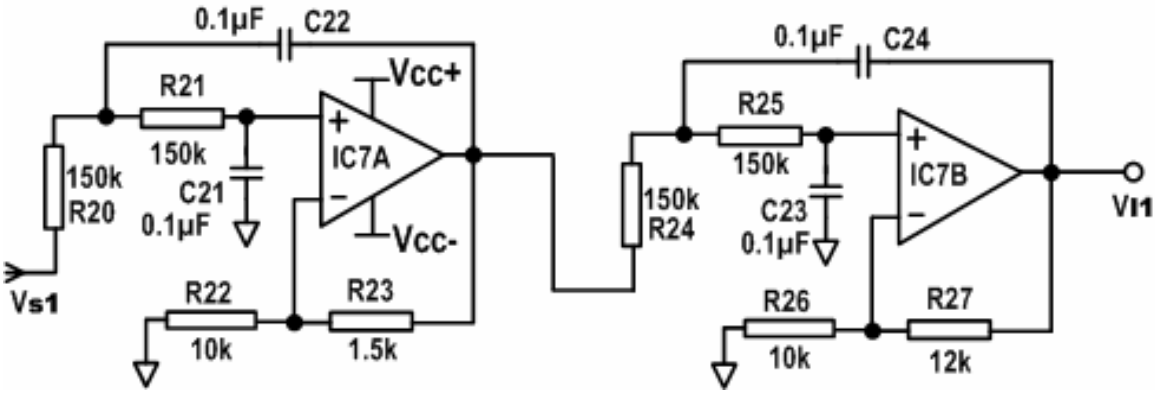

Fig. 3.7 (a) Fourth order Butterworth low pass filter
(IC7A, IC7B: TL084).

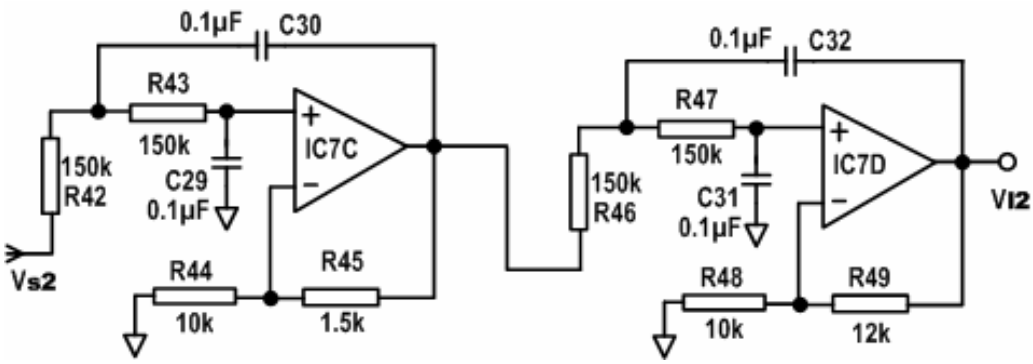

Fig. 3.7 (b) Fourth order Butterworth low pass filter
(IC7C, IC7D: TL084).

3.2.5 AC/DC separator

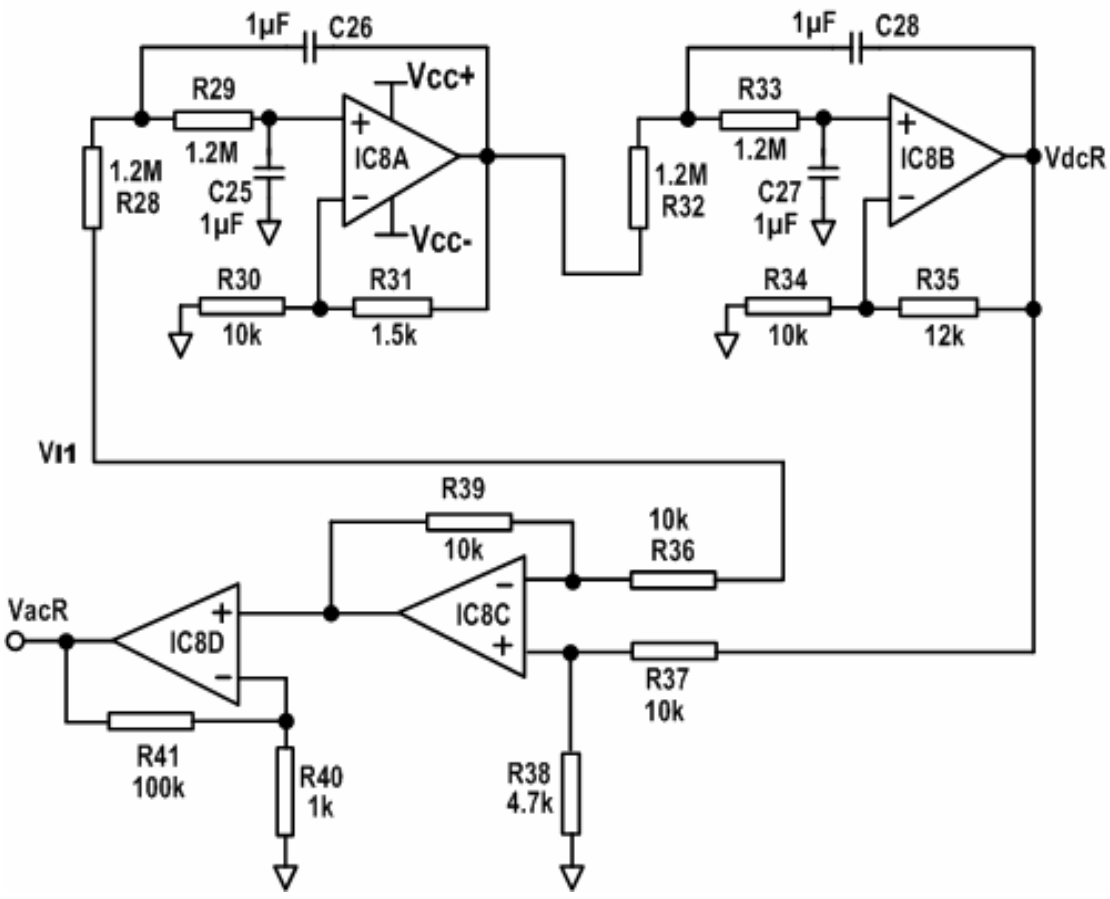

Fig. 3.8 (a) Fourth order Butterworth LPF (DC separation) with AC/DC separator.
(IC8A, IC8B, IC8C, IC8D: TL084).

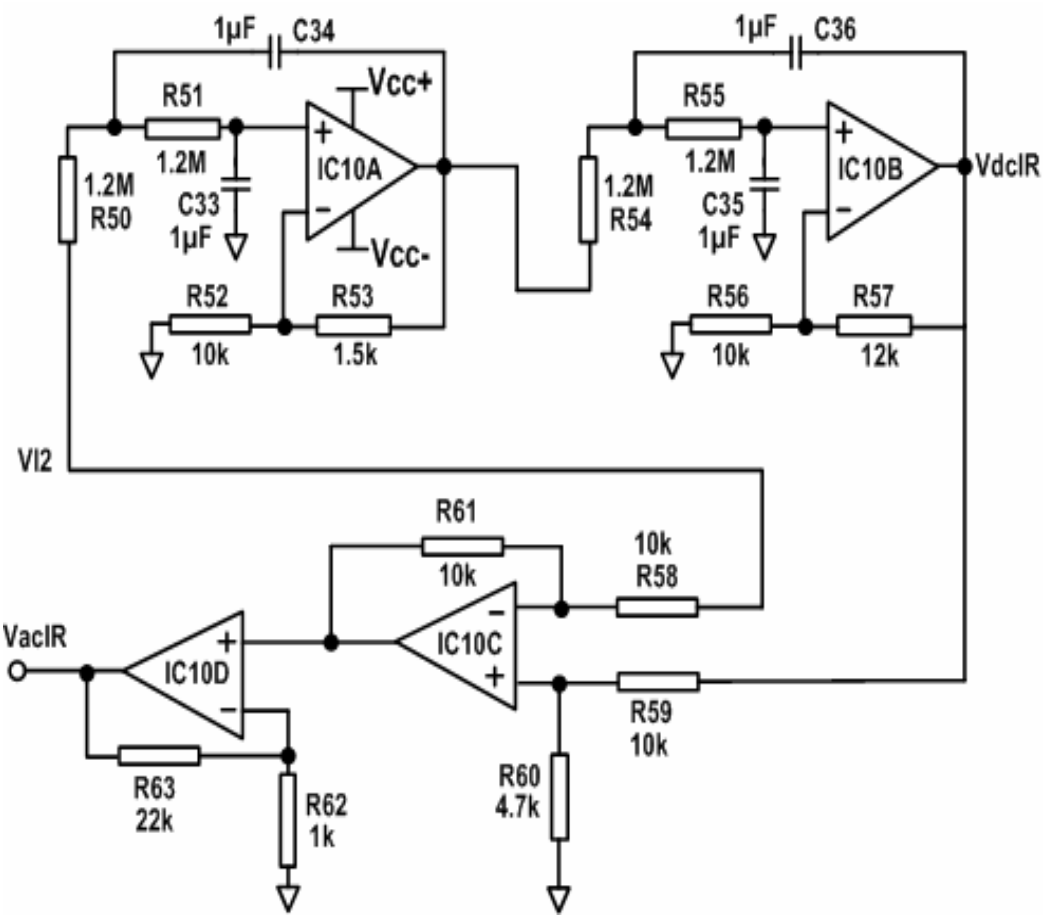

Fig. 3.8 (b) Fourth order Butterworth LPF (DC separation) with AC/DC separator. (IC10A, IC10B, IC10C, IC10D: TL084).

The output of the low pass filter is a clean plethysmographic signal but consists of both AC and DC parts. So the AC and DC components should be separated out in order to calculate the R/IR ratio. The DC parts are obtained by another fourth order Butterworth low pass filter with a cut off frequency of 0.1 Hz. The DC values are then subtracted from total signal to get AC signal. The subtraction is done by using a differential amplifier. The gain of the differential amplifier is kept as 1. Fig 3.8 shows a circuit diagram of fourth order Butterworth LPF with AC/DC separator for infrared signal. The expression for calculating the gain is $A = 1+R_f/R_i$, where $R_f = R_{23}$, R_{27}, R_{31}, R_{35}, R_{39}, R_{41}, $Ri = R_{22}$, R_{26}, R_{30}, R_{34}, R_{36}, R_{40}. For the cut off frequency it is $f_c = 1/ 2\pi\sqrt{R_1R_2C_1C_2}$, where $R_1 = R_{20}$, R_{24}, R_{28}, R_{32}; $R_2 =$, R_{21}, R_{25}, R_{29}, R_{33}, $C_{21} = C_{22} = C_{23} = C_{24}$, $C_{25} = C_{26} = C_{27} = C_{28}$.

3.3 Control and display unit

In this design, as represented in Fig. 3.1, the control and display unit has been developed using two microcontrollers one for timing and control unit and the other for acquisition, processing and display unit. This has been done, primarily for flexibility in H/W development and convenience in programming. For more compact circuit, the design can be later modified to have a single μC for both the function. The timing and control unit uses a 20 pin (AT89C2051) microcontroller for generating the controls for the signal conditioning unit. It has been programmed using 8051 assembly language. Interfacing of AT89C2051 microcontroller as timing pulse controller is shown in Fig. 3.9. The acquisition, processing and display unit which uses an 8-bit microcontroller as its core of the ADuC812. The ADuC812 consists of micro-converter with multi-channel 12 bit ADC, embedded MCU and other additional features on a single chip [22]. The acquisition, processing and display unit consists of the ADuc812, serial port and a LCD display. The main function of this unit is to digitize the analog signals using the in-built ADC. The digitized values are used for the calculation of the R/IR ratio, which is used for the calculation of the oxygen saturation. The value of the oxygen saturation being obtained is displayed using a LCD display. The ADC, serial port and the display unit are controlled using the microcontroller. The function of the acquisition, processing and display unit is described in the following subsection.

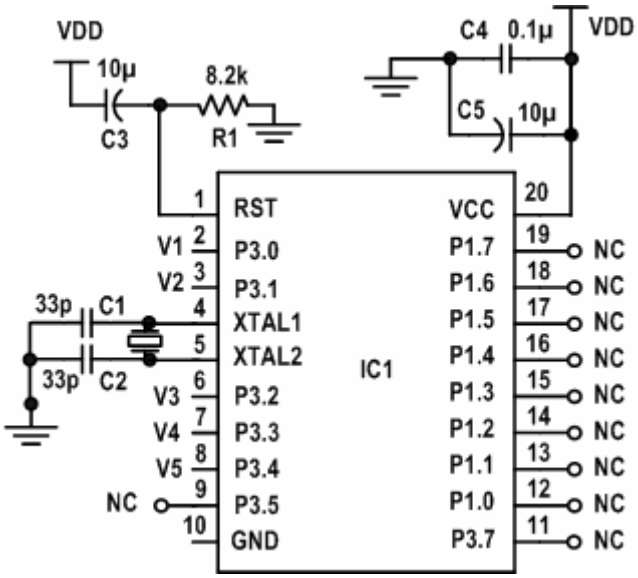

Fig. 3.9 Interface of IC1 (AT89C2051) as the timing pulse controller.

3.3.1 Microcontroller ADuC812

This microcontroller has on-chip ADC and 8052 compatible microcontroller. The ADC conversion block incorporates fast, multi-channel, 12-bits, single supply A/D converter. This block consists of multi-channel multiplexer, track/hold, on-chip reference, calibration features and A/D converter.

The ADC consists of successive-approximation converter. The converter's analog input range is 0 V to V_{REF}. A high precision, low drift and factory calibrated 2.5 V reference is provided on-chip [22]. The internal reference may be overdriven via the external V_{REF} pin. This external reference can be in the range of 2.3 V to AVDD. In this application Timer 2 is used to generate a repetitive trigger for ADC conversions with a sampling rate of 100 Sa/s. The analog signals that are obtained from the signal conditioning unit are given to the ADC. All the components in the ADC block are easily configured via the SFR interface from the core MCU. The digitized values obtained are then processed for the calculation of the R/IR ratio. After which the oxygen saturation value can be obtained. Description on ADC functioning is given in Appendix A.

At its core, the ADuC812 incorporates a high performance 8-bit (8052 compatible) MCU with on-chip reprogrammable nonvolatile Flash program memory controlling a multi-channel (eight input channels) 12-bit ADC. This microcontroller has 32 programmable I/O lines, three 16 bit timer/counter, nine interrupts sources, two priority levels and 8051 compatible instruction set. The unit also controls the serial port and the LCD display. It calculates the R/IR ratio and determines the oxygen saturation value using Eqn. 2.7 and these data are displayed using a LCD display.

The microcontroller has in-circuit serial download access. For level translation while downloading code from a PC, the ADuC812's UART requires an external RS-232 chip. In addition to the basic UART connections, the chip needs to be triggered into download mode. A 1 k pull-down resistor is connected as in Fig. 3.10 that can be connected to the PSEN pin through a jumper. To get the ADuC812 into download mode, the jumper is connected and powercycle the device such that a new program is received serially. With the jumper removed, the device will come up in normal mode (and execute the program) whenever power is cycled or RESET is toggled. PSEN is normally an output, and is sampled as an input only on the falling edge of RESET. No external signals should be capable of pulling the PSEN pin low, except the jumper which is used for programming [22].

3.3.2 Display

The display used is 2 lines x 16 characters LCD display with its controller. It works on a single 5 V supply. The hardware interface of the display consists of 8 data lines and 3 control lines (RS, R/$\overline{W}$, $\overline{EN}$), which are controlled using a microcontroller as shown in Fig. 3.10. Control pin R/$\overline{W}$ is used for writing data/control word or reading the status of the display. The RS control pin is used to distinguish between 8-bit data word and control word that is sent to the display. The data are latched on falling edge of the pulse $\overline{EN}$. Data bit 7 is monitored for logic high (busy) to ensure that the display is not overwritten. The RxD and TxD lines of port pins P3.0 and P3.1 are used for serial communication with PC.

3.3.3 Microcontroller interfacing

Fig. 3.10 shows the system configuration. The capacitor values are taken as 0.01 μF, except the capacitors connected to the crystal is 33 pF each. Pins 1 to 4 are the ADC channel. For accurate ADC operation, the voltage applied to V_{REF} must be between 2.3 V to $AV_{DD,}$ below which it can result in missing codes and non-monotonicity. For downloading code from a PC, external RS-232 chip for level translation is connected to the ADuC812's UART through a 9-pin connector as shown in Fig. 3.10. The connection of various port pins of the microcontroller of ADuC812 are given in Table 3.2.

Table 3.2 Functions of the various port pins of the ADuC812 microcontroller used for acquisition, processing and display unit.

I/O Port Pins	Functions
P0	8-bit data lines, display.
P2.0	R/W of the display.
P2.1	RS of the display.
P3.2	EN of the display.

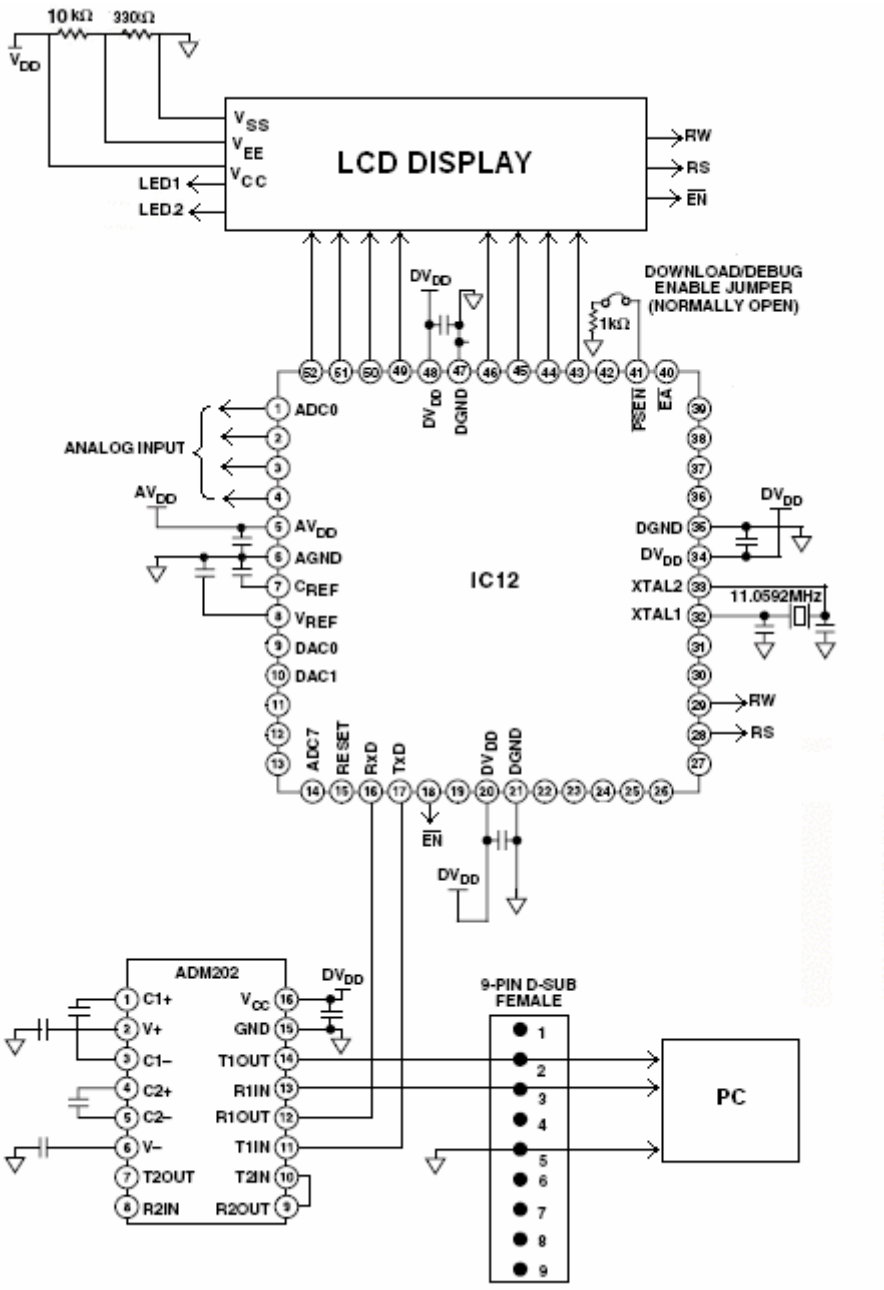

Fig. 3.10 Interface of the IC12 (ADuC812) to various circuits [22].

Chapter 4

SOFTWARE DESCRIPTION

4.1 Introduction

The software has been developed using 8051 assembly language. A program on AT89C2051 (IC1 in Fig. 3.9) generates control and timing pulses. Another program on ADuC812 (IC12 in Fig. 3.10) carries out the signal acquisition, processing and result display. This chapter provides a description of the control of the hardware blocks by the program on the microcontroller, implementation of the processing, and overall operation.

4.2 Generation of timing and control pulses

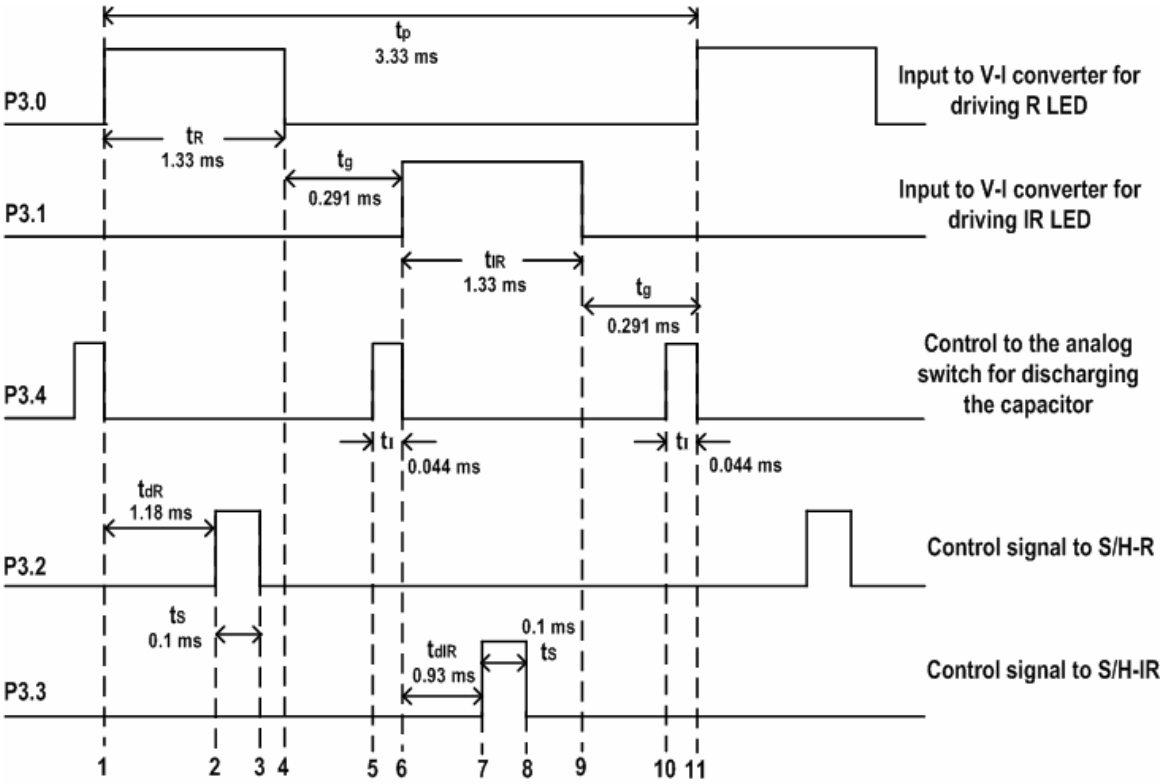

Fig. 4.1 Timing and control pulses.

Generation of all the timing and control pulses, as shown in Fig. 4.1, are handled by program "`oxy_tac`", written in assembly language, on the microcontroller AT89C2051 (IC1 in Fig. 3.9). Time intervals are measured using Timer-1 of the μC by loading a count

$$N = 65536 - t_p f_c/12 \qquad (4.1)$$

where, t_p = time interval in μs

f_c is the microcontroller crystal frequency in MHz.

Each time the timer overflows, a new count for the next time interval is loaded and the control signals (port pins) are pulled high or low as required.

It was decided to sample the arterial pulse by pulsing the light sources at ≈ 300 Hz, and Fig. 4.1 gives the various pulse timings used for this sampling rate. For light pulse rate of 300 Hz and f_c = 12 MHz, the count for the time duration in Fig. 4.1 are given in Table 4.1

Table 4.1 Shows the count for the time duration given in Fig. 4.1.

Interval	Time duration (ms)	Count
1–2	1.18	64356
2–3	0.1	65436
3–4	0.05	65486
4–5	0.291	65245
5–6	0.044	65492
6–7	0.93	64606
7–8	0.1	65436
8–9	0.3	65236
9–10	0.291	65245
10–11	0.044	65492

4.3 Signal acquisition

Signal acquisition is done using the four input channels of the ADC. Two of the channels are for the DC components and the other two are for the AC components of the red and

the infrared signals respectively. From the acquired waveform, the R/IR ratio is first calculated which is then used in the calculation of the oxygen saturation using Eqn. 2.7, based on photon diffusion analysis. All calculations are handled by program "`oxy_apd`", written in assembly language, on the microcontroller ADuC812 (IC12 in Fig. 3.10). All the results are displayed on the LCD display.

A sampling rate of 100 Sa/s is used. The acquired signals have certain AC components and the acquired AC signals may have DC offsets. We have used digital processing of the acquired signals to find the average for DC value and peak-to-peak for AC value.

The average, peak, and valley are calculated based on a method used earlier for processing of impedance glottograph waveform [23]. The average $a(n)$ is calculated by using first order IIR low pass filter [23] on the input PPG waveform $x(n)$

$$a(n) = \alpha a(n-1) + (1-\alpha)x(n) \tag{4.2}$$

For peak $p(n)$ detection, the waveform is first rectifier detected and averaged with a fast attack response towards the new input and slow release response towards the average.

$$\begin{aligned} p(n) &= \beta\, p(n-1) + (1-\beta)x(n) && \text{for } x(n) \geq p(n-1) \\ &\gamma\, p(n-1) + (1-\gamma)a(n) && \text{otherwise} \end{aligned} \tag{4.3}$$

First difference of this waveform is used for slope detection, and the sample with up to down slope change is taken as the peak.

For valley detection , a similar processing is done except that the rectification direction is reversed.

$$\begin{aligned} v(n) &= \beta\, v(n-1) + (1-\beta)x(n) && \text{for } x(n) \leq v(n-1) \\ &\gamma\, v(n-1) + (1-\gamma)a(n) && \text{otherwise} \end{aligned} \tag{4.4}$$

Values α, β, γ should be selected to give acceptable dynamic response and low ripple. If α is reduced, the average has too much ripples as it follows the input. In Eqn.

4.3, the γ value is used for the peak detection. If it is decreased, the waveform has a fast roll off and almost follows the input which may lead to false peak detections. If it is increased, the peak detection decays slowly and may miss some of the peaks in the input. If the factor β is increased, the waveform does not follow the input and thus, leads to false detections of peak.

For first order IIR filter of Eqn. 4.2, the 99 % rise time for unit step input is given as

$$T_{0.99} = \left(-2/\log\alpha - 1\right)/f_s$$

With sampling rate of 100 Sa/s, we have selected α = 0.998, β = 0.5 and γ = 0.996 and for 99 % rise time, these correspond to 23 s, 66 ms and 11 s. Response time and smoothening by using these values were verified by offline processing of the waveforms, using MATLAB implementation of Eqn. 4.2, 4.3, and 4.4.

Average of the dc input is taken as the dc value I_0 and peak-to-peak of the ac input is taken as the ac value ΔI_0. All computations are carried out using 16-bit (2-byte) representation for coefficients and all the equations along with the coefficients are implemented accordingly. The equations for average (A), peak (P) and valley (V) for the above given values of α, β, and γ after scaling for 16-bit computation are

$$A(n) = \left(4092 \times A(n-1) + 4 \times X(n)\right) \times 2^{-12} \tag{4.5}$$

$$P(n) = \begin{cases} \left(410 \times P(n-1) + 3686 \times X(n)\right) \times 2^{-12} & \text{for } X(n) \geq P(n-1) \\ \left(4035 \times P(n-1) + 61 \times A(n)\right) \times 2^{-12} & \text{otherwise} \end{cases} \tag{4.6}$$

$$V(n) = \begin{cases} \left(410 \times V(n-1) + 3686 \times X(n)\right) \times 2^{-12} & \text{for } X(n) \leq V(n-1) \\ \left(4035 \times V(n-1) + 61 \times A(n)\right) \times 2^{-12} & \text{otherwise} \end{cases} \tag{4.7}$$

The program has a main part and an interrupt service routine (ISR), which invoked periodically every sampling interval by programming Timer-2. Inputting the values and sample-by-sample processing, for peak and valley detection are handled in the ISR.

The interrupt service routine can be summarized as the following

Acquire V_{dcR}, V_{acR}, V_{dcIR}, V_{acIR} from ADC inputs

Calculate average for all the four inputs using Eqn. 4.5.

Calculate +ve rectified average for V_{acR}, and V_{acIR} using Eqn. 4.6, for peak detection and find 2-point slope.

Calculate –ve rectified average for V_{acR}, and V_{acIR} using Eqn. 4.7, for valley detection and find 2-pont slope.

For peak picking of V_{acR} input, let us say $X_R(n)$ represents the 16-bit integer input. We use variables $P_R(n)$, $f_{PR}(n)$, and $P_{mR}(n)$ in the peak picking process. $P_R(n)$, is the +ve rectified average output after processing $X_R(n)$ using Eqn. 4.6. The peak picking process returns the peak value $P_{mR}(n)$ which is the new peak value or earlier detected peak. Flag $f_{PR}(n)$ indicates the slope. It is 1 if the values are increasing and 0 if the values are decreasing. A 1-to-0 transition indicates occurrence of a peak. The peak picking process can be described as the following,

If $X_R(n) \geq P_R(n-1)$, then

$f_{PR}(n) = 1,\ P_{mR}(n) = P_{mR}(n-1)$

else

if $f_{PR}(n-1) = 1,$ then

$P_{mR}(n) = P_R(n-1)$

else $P_{mR}(n) = P_{mR}(n-1)$

$f_{PR}(n) = 0$

For picking the valleys from V_{acR} input, let us say $X_R(n)$ represents the 16-bit integer input. We use variables $V_R(n)$, $f_{VR}(n)$, and $V_{mR}(n)$ in the peak picking process. $V_R(n)$, is the –ve rectified average output after processing $X_R(n)$ using Eqn. 4.7. The valley picking process returns the valley value $V_{mR}(n)$ which is the new peak value or earlier detected valley. Flag $f_{VR}(n)$ indicates the slope. It is 1 if the values are decreasing and 0 if the values are increasing. A 1-to-0 transition indicates a valley detection. The valley picking process is as follows

If $X_R(n) \le V_R(n-1)$, then

$f_{VR}(n) = 1,\ V_{mR}(n) = V_{mR}(n-1)$

else

if $f_{VR}(n-1) = 1,$ then

$V_{mR}(n) = V_R(n-1)$

else $V_{mR}(n) = V_{mR}(n-1)$

$f_{VR}(n) = 0$

Similar procedure is used for picking the peak and valley for V_{acIR} input.

It is to be noted that for all the variables, we are storing the immediate past sample, and processing with present input and past outputs and flags, because all the filters are 1st order IIR filters. For the picked peak and valley values, we store the current output and the last four outputs, for 5-point median filtering for further smoothening these values.

In the main program, the slope flags for the peak and valley of the red and infrared inputs are checked. If a particular peak or valley is detected, the corresponding array is updated with the new value. The array is copied to a sorting buffer and the median is found. The median values are given as

M_{PR} = median $\{P_R(n), P_R(n\text{-}1), P_R(n\text{-}2), P_R(n\text{-}3), P_R(n\text{-}4)\}$

M_{PIR} = median $\{P_{IR}(n), P_{IR}(n\text{-}1), P_{IR}(n\text{-}2), P_{IR}(n\text{-}3), P_{IR}(n\text{-}4)\}$

M_{VR} = median $\{V_R(n), V_R(n\text{-}1), V_R(n\text{-}2), V_R(n\text{-}3), V_R(n\text{-}4)\}$

M_{VIR} = median $\{V_{IR}(n), V_{IR}(n\text{-}1), V_{IR}(n\text{-}2), V_{IR}(n\text{-}3), V_{IR}(n\text{-}4)\}$

Next the peak-to-valley differences are calculated as given below

$$\Delta I_R = M_{PR} - M_{VR}$$

$$\Delta I_{IR} = M_{PIR} - M_{VIR}$$

and we take the average value as DC values

$$I_R = A_R(n)$$
$$I_{IR} = A_{IR}(n)$$

We calculate the ratio *r* of AC/DC ratios for red and infrared as per Eqn. 2.6

$$r = \frac{(\Delta I_R / I_R)}{(\Delta I_{IR} / I_{IR})} \tag{4.8}$$

To maintain precision in calculations, we calculate $R = 100\ r$ as the following

$$R = \frac{10 \times [(100 \times \Delta I_R)/I_R]}{(100 \times \Delta I_{IR})/I_{IR}} \tag{4.9}$$

and calculation of SaO_2 as per Eqn. 2.7 (based on photon diffusion analysis) is given below

$$\mathrm{SaO}_2 = \frac{r\sigma_{a,IR}^{0\%} - K_r' \sigma_{a,R}^{0\%}}{K_r'\left(\sigma_{a,R}^{100\%} - \sigma_{a,R}^{0\%}\right) + r\left(\sigma_{a,IR}^{0\%} - \sigma_{a,IR}^{100\%}\right)}$$

where, the coefficients values are selected as given in [12],

$\sigma_{a,R}^{100\%} = 0.036\ \mu m^2$, $\sigma_{a,R}^{0\%} = 0.355\ \mu m^2$, $\sigma_{a,IR}^{100\%} = 0.134\ \mu m^2$, $\sigma_{a,IR}^{0\%} = 0.080\ \mu m^2$,

$K_r' = 1.56$.

After substituting these values in Eqn. 2.7 we have

$$\mathrm{SaO}_2 = \frac{(r \times 0.08 - 0.55517)}{(-0.499 - r \times 0.06)} \tag{4.10}$$

For percentage SaO_2 calculation we use $R = 100\ r$ and now we get,

$$\%\,\mathrm{SaO}_2 = \frac{(55517 - R \times 800)}{(499 + R \times 6)} \tag{4.11}$$

The percentage oxygen saturation is displayed in a LCD display. The flowchart for calculation of SaO_2 is given in Fig. 4.2. The main program basically carries out SaO_2 calculation. This process is periodically interrupted by Timer-2. This ADC inputs are handled. After each ISR, the main calculation proceeds from the place where it was interrupted. Hence in a given calculation, the values used may come from different execution of ISR.

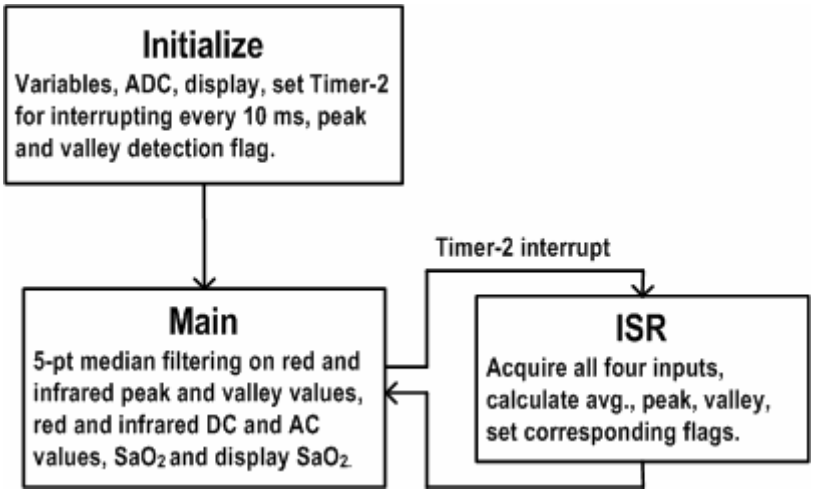

Fig. 4.2 Flowchart for calculation of SaO_2.

Chapter 5

VALIDATION OF THE HARDWARE AND TEST RESULTS

5.1 Introduction

The hardware was tested section wise under various conditions using test signals to validate its functions. All the testing was done with opamps being powered at ±5 V and the microcontroller at +5 V.

5.2 Voltage-to-current converter

The performance of the voltage-to-current converter circuit of Fig. 3.4 has been tested by applying dc voltages from 0V to +5 V with different resistive loads (R_L) in place of the LED's. The test results are given in Table 5.1. From Table 5.1 the output current for driving the red LED is around 22 mA and for the infrared LED, it is around 13 mA and is almost constant even with change in R_L.

Table 5.1 Performance of the V-I converter in Fig. 3.4 with R_{11} = 68 Ω, R_5 = 22 KΩ, R_L = 10 Ω, 15 Ω, and 22 Ω.

V_1 (V)	V_2 (V)	R_L = 10 Ω		R_L = 15Ω		R_L =22 Ω	
		I_r (mA)	I_{ir} (mA)	I_r (mA)	I_{ir} (mA)	I_r (mA)	I_{ir} (mA)
1.0	0	5.6	0	5.0	0	4.7	0
2.0	0	9.1	0	8.1	0	9.1	0
3.0	0	12.8	0	13.4	0	13.7	0
4.0	0	18.1	0	18.4	0	18.0	0
5.0	0	22.0	0	21.6	0	22.8	0
0	1.0	0	2.4	0	2.0	0	2.0
0	2.0	0	5.0	0	6.0	0	5.4
0	3.0	0	9.1	0	8.1	0	8.5

0	4.0	0	11.3	0	12.1	0	12.1
0	5.0	0	12.4	0	12.9	0	12.9

5.3 Integrator

The performance of integrator of Fig. 3.5 was evaluated and the test results are given in Table 5.2. The testing was done by injecting a controlled current with a variable dc source and a high value resistance simulating the output of the photodiode as shown in Fig. 5.1. The instantaneous output voltage of the circuit was observed after a fixed interval of time, which in turn reflected the amount of voltage that can be obtained at the output when a fixed current flows for a fixed amount of time. The sensitivity of the integrator with different *R* value is shown in Fig. 5.2.

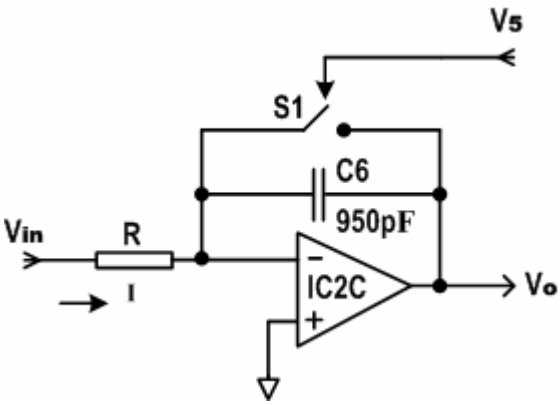

Fig. 5.1 Circuit for testing the integrator (IC2C: TL084).

Table 5.2 Test results for the integrator in Fig. 5.1, with t = 1.78 ms.

V_{in} (V)	R = 2.2 MΩ		R = 4.7 MΩ		R = 6.8 MΩ	
	V_o (V)	V_{in}/It(V/μA.ms)	V_o (V)	V_{in}/It(V/μA.ms)	V_o (V)	V_{in}/It(V/μA.ms)
1.0	0.78	0.962	0.40	1.052	0.27	1.031
2.0	1.54	0.952	0.80	1.052	0.54	1.031
3.0	2.34	0.963	1.18	1.040	0.82	1.044
4.0	3.12	0.965	1.60	1.056	1.10	1.050
5.0	3.90	0.962	1.98	1.044	1.38	1.054

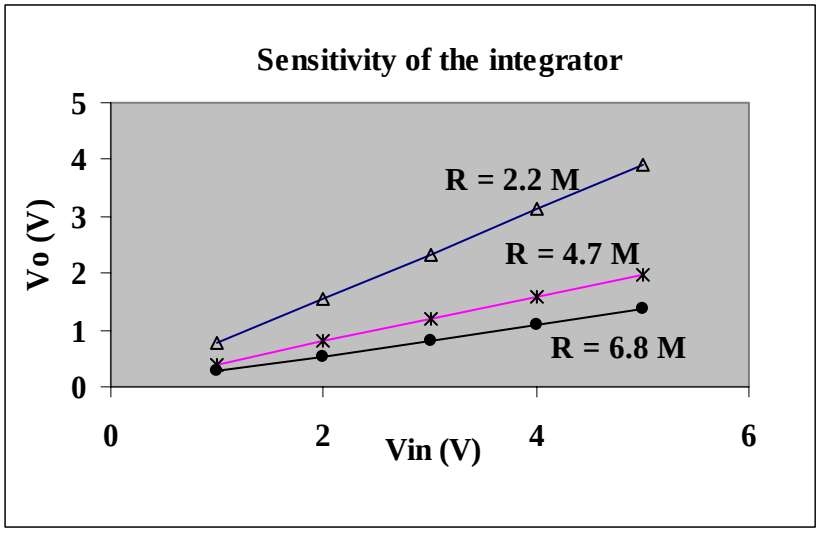

Fig. 5.2 Sensitivity of the integrator circuit.

5.4 Low pass filter

The performance of the low pass filter of Fig. 3.8, with cut off frequency of 41 Hz has been studied using sine wave as input signal with frequency (f) ranging from 1 Hz to 200 Hz, and the output voltage ($V_{o(p\text{-}p)}$) was observed. The test results are given in Table 5.3. The magnitude response of the filter is shown in Fig. 5.3.

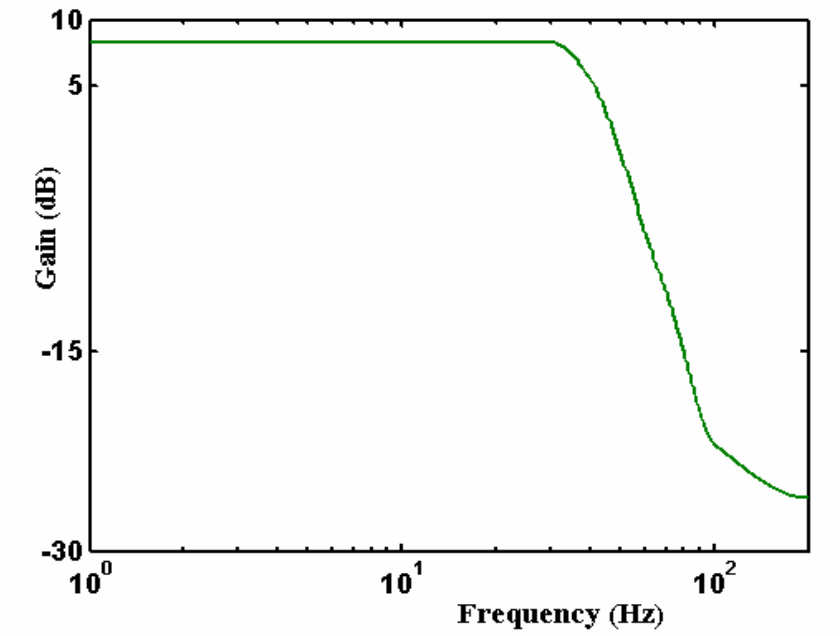

Fig. 5.3 Magnitude response of the low pass filter.

Table 5.3 Frequency response of the filter with Vin = 1.0 $V_{(p\text{-}p)}$.

f (Hz)	$V_{o(p\text{-}p)}$
1	2.6
5	2.6
10	2.6
20	2.6
20	2.6
30	2.6
40	1.9
50	1.0
60	0.5
70	0.3
80	0.2
90	0.1
100	0.08
200	0.05

5.5 Analog-to-digital converter

The analog-to-digital converter of ADuC812 has been tested for its linearity and crosstalk between the channels. For testing linearity, two channels were shorted and DC voltages within the input range of the ADC were applied. The outputs in BCD (D_{out1} and D_{out2}), were found to be almost comparable to the expected values as given in Table 5.4. Fig. 5.4 gives the plot between V_{in} and D_{out1} and D_{out2}. The two outputs are almost equal. And for checking the crosstalk, one channel (V_{in1}) was grounded and the other channel (V_{in2}) was given a DC voltage, and vice versa. The results were displayed in BCD and are given in Table 5.5. Table 5.6 shows the test results for the calculation of the AC/DC value.

Table 5.4 Test results for evaluation of linearity.

V_{in} (V)	V_{in} (BCD)	D_{out1}	D_{out2}
0.2	327	235	228
0.3	491	447	439
0.5	819	766	757

0.8	1310	1262	1254
1.0	1638	1578	1568
1.2	1966	1912	1902
1.5	2457	2387	2381
1.8	2949	2871	2864
2.0	3276	3197	3190
2.2	3604	3514	3509
2.4	3932	3867	3860

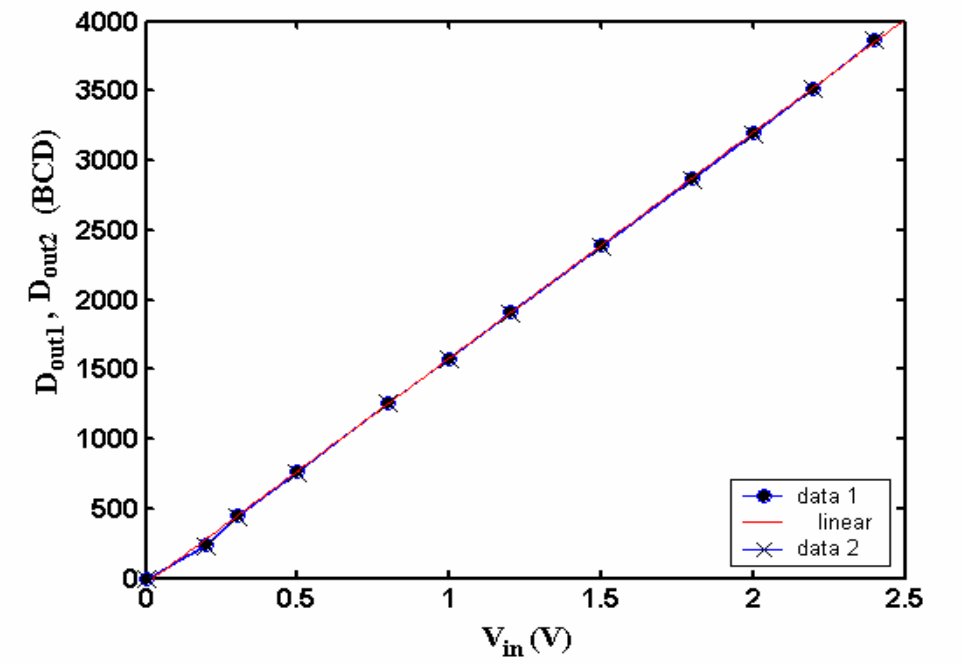

Fig. 5.4 Plot between V_{in} and D_{out1} and D_{out2}.

Table 5.5 Test results for evaluation of crosstalk (i) with V_{in1} grounded.

V_{in1} (V)	V_{in2} (V)	V_{in1} (BCD)	V_{in2} (BCD)	D_{out1}	D_{out2}
0	0.2	0	327	0	240
0	0.5	0	819	0	755
0	0.8	0	1310	0	1277
0	1.0	0	1638	0	1590
0	1.5	0	2457	0	2370
0	2.0	0	3276	0	3194

(ii) with V_{in2} grounded

V_{in1} (V)	V_{in2} (V)	V_{in1} (BCD)	V_{in2} (BCD)	D_{out1}	D_{out2}
0.2	0	327	0	239	0
0.5	0	819	0	752	0
0.8	0	1310	0	1229	0
1.0	0	1638	0	1583	0
1.5	0	2457	0	2355	0
2.0	0	3276	0	3200	0

Table 5.6 Test results for the calculation of the AC/DC value.

DC (V)	*AC* (V_{pp})	Expected (AC/DC)	*DC′* (BCD)	*AC′* (BCD)	Observed (AC/DC)
2.0	0.5	25	3243	633	19
1.0	0.5	50	1555	634	40
2.0	1.0	50	3240	1495	46
2.0	1.5	75	3230	2347	72
0.5	0.5	100	771	634	83
1.0	1.0	100	1562	1493	93
2.0	2.0	100	3229	3126	96
1.0	1.5	150	1566	2359	150
0.5	1.0	200	767	1501	195
1.0	2.0	200	1559	3130	200
0.5	1.5	300	767	2357	307
0.5	2.0	400	784	3126	399

5.6 Test results

Testing of individual blocks was carried out. The results are discussed in this section.

Fig. 5.5 shows the various control signals that are generated by the microcontroller for controlling the signal conditioning unit. The output from the sensor circuit is given in Fig.5 6. This output is sampled and held as shown in Fig. 5.7. Low pass filtering is done and the output contains the AC and DC components, this is shown in Fig.

5.8. Fig. 5.9 shows the AC and DC signals with respect to red and infrared light respectively.

Test signals were used for the calculation of SaO_2. First, the peaks and valleys were calculated, after which the maximum and minimum point were calculated. 5-point median filtering was implemented in the program, because of the fluctuations in the maximum and minimum values. The R/IR ratio was calculated using Eqn.2.6.

Control pulse for driving R LED **V_1**

Control pulse for S/H-R **V_3**

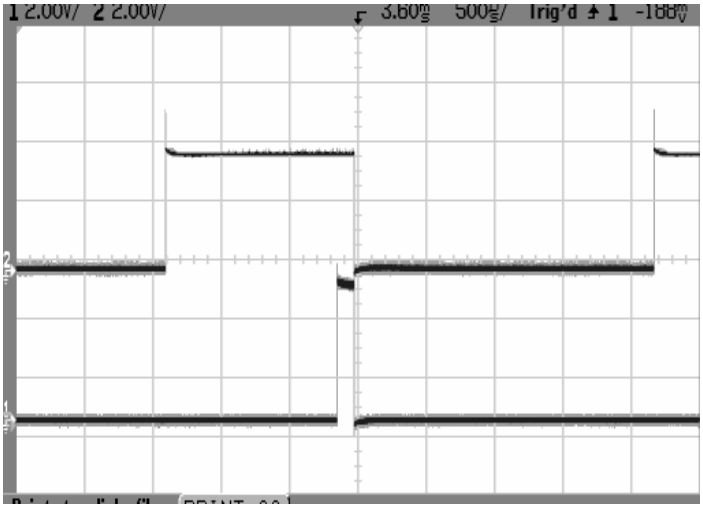

Control pulse for driving IR LED **V_2**

Control pulse for S/H-IR **V_4**

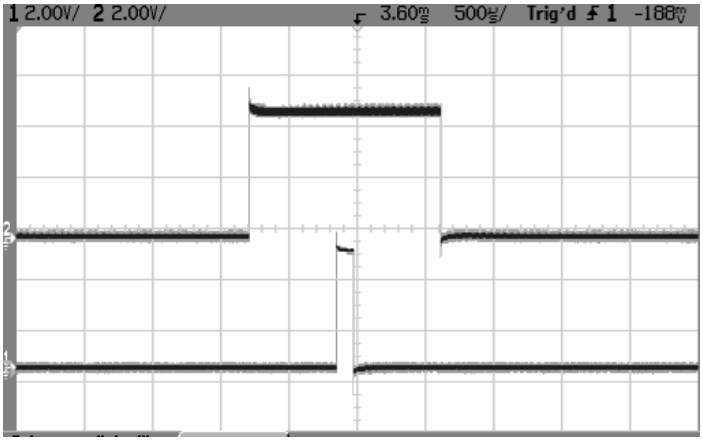

Control pulse for discharging the capacitor **V_5**

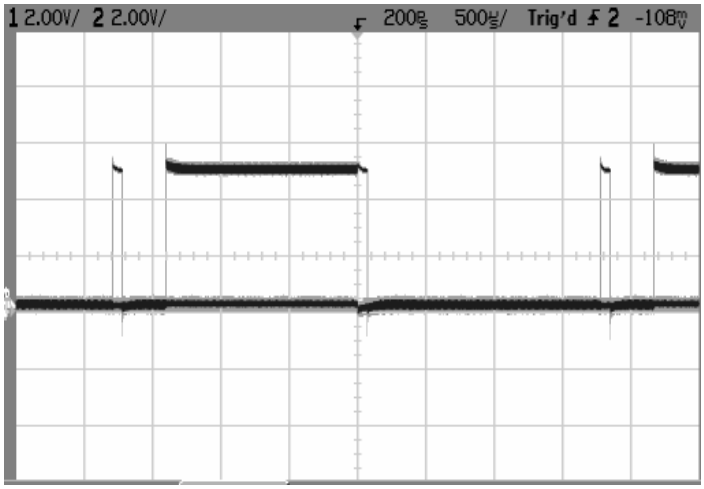

Fig. 5.5 Control signals from the microcontroller port pins.

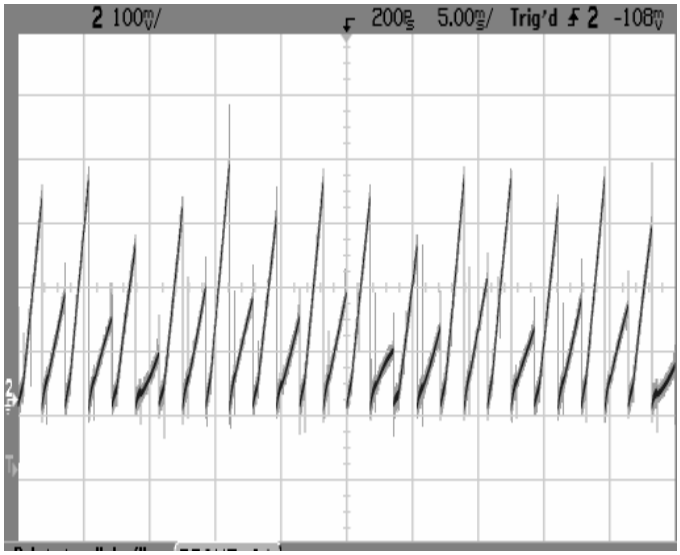

Fig. 5.6 Output waveform from the integrator (Plain reflection/pick up by red (lower amplitude)and infrared (higher amplitude) LED's and photodiode).

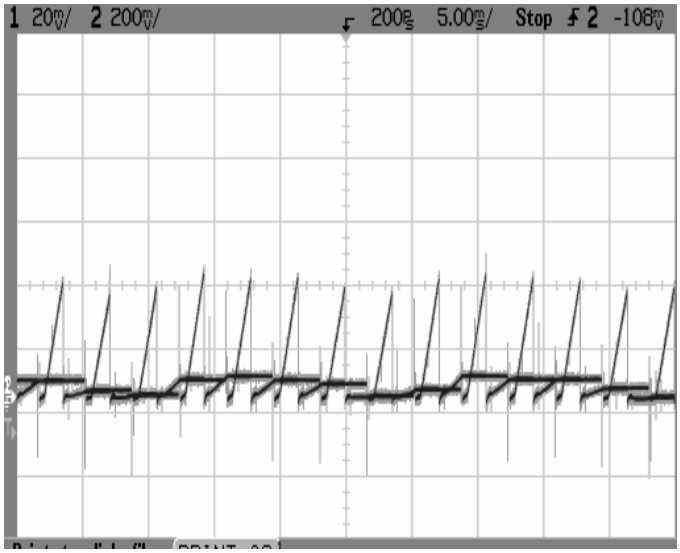

Fig. 5.7 Output waveform from S/H circuit for the red.

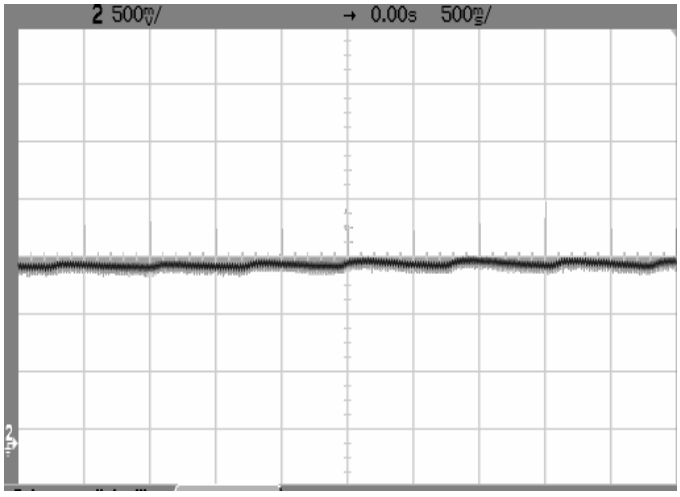

Fig. 5.8 AC+DC ir signal from fourth order Butterworth LPF.

DC signal corresponding to IR signal

AC signal corresponding to IR signal

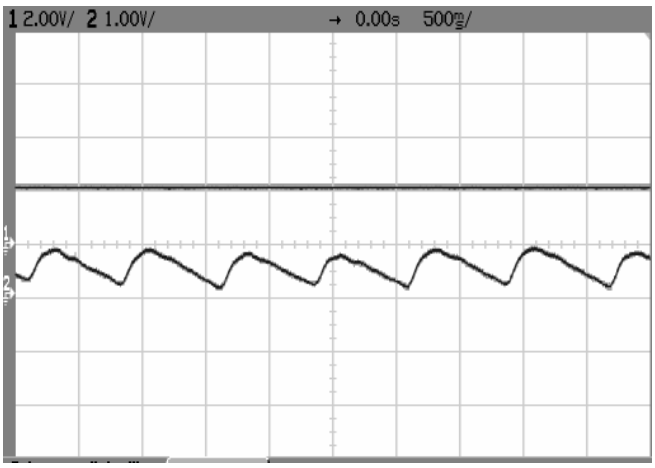

Fig. 5.9 (a) Output waveforms from AC/DC separator with respect to infrared (IR).

DC signal corresponding to R signal

AC signal corresponding to R signal

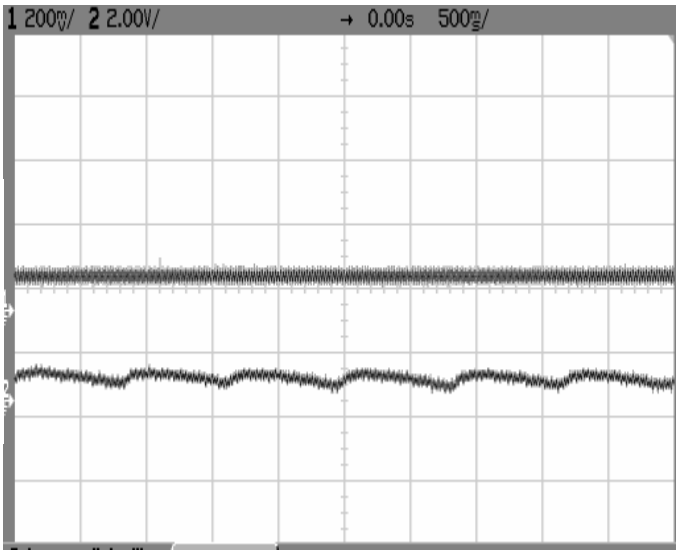

Fig. 5.9 (b) Output waveforms from AC/DC separator with respect to red (R).

Chapter 6
SUMMARY AND CONCLUSIONS

6.1 Summary of work done

The aim of this project was to develop a pulse oximeter which can be used in cardiovascular diagnosis setup by making use of previous designs and making appropriate modifications. Two microntrollers have been used, one for controlling the signal conditioning unit and the other one a built-in multichannel ADC for controlling the acquisition, processing and display unit. The analog part of the instrument to acquire stable plethysmograms has been developed which is controlled using a microcontroller. Assembly language program was written and implemented for the calculation of SaO_2. The software has been tested using test signals. These test signals have been processed and the average, peak, and valley were calculated and verified with the desired results. 5-point median filtering was done on the picked peaks and valleys. Then the AC/DC ratios for the red and infrared were calculated, and the calculation of percentage arterial oxygen saturation is done. The calculated value is displayed on a LCD.

6.2 Suggestions for future work

Further modification can be done on the hardware, by using single microcontroller for controlling both the functions. A provision can be made to vary the light intensity dynamically for different subjects by providing a feedback control. The instrument has to be validated by taking large number of recordings and comparing the readings with those from a standard instrument.

Appendix A
DESCRIPTION OF ADC FUNCTIONING

The ADC consists of a conventional successive-approximation converter. Single step or continuous conversion modes can be initiated in software or alternatively by applying a convert signal to an external pin. Timer 2 can also be configured to generate a repetitive trigger for ADC conversions. The ADC core contains internal offset and gain calibration registers [22].

The equivalent circuit of the analog input section is shown in Fig. A.1. Each ADC conversion is divided into two distinct phases as defined by the position of the switches in Fig. A.1. During the sampling phase (with SW1 and SW2 in the "track" position), a charge proportional to the voltage on the analog input is developed across the input sampling capacitor. During the conversion phase (with both switches in the "hold" position), the capacitor DAC is adjusted via internal SAR logic until the voltage on node A is zero, indicating that the sampled charge on the input capacitor is balanced out by the charge being output by the capacitor DAC. The digital value finally contained in the SAR is then latched out as the result of the ADC conversion. Control of the SAR, and timing of acquisition and sampling modes, is handled automatically by built-in ADC control logic. Acquisition and conversion times are also fully configurable under user control [22].

Whenever a new input channel is selected, a residual charge from the 2 pF sampling capacitor places a transient on the newly selected input. The signal source must be capable of recovering from this transient before the sampling switches click into "hold" mode. Delays are implemented in software to account for input stage settling. We can choose a very fast settling op amp to drive each analog input in hardware implementation. A better solution is using any amplifier, as shown in Fig. 11. The R/C circuit in Fig. A.2 helps in removing some incoming high frequency noise, but its primary function is to ensure that the transient demands of the ADC input stage are met. It does so by providing a capacitive bank from which the 2 pF sampling capacitor can draw its charge.

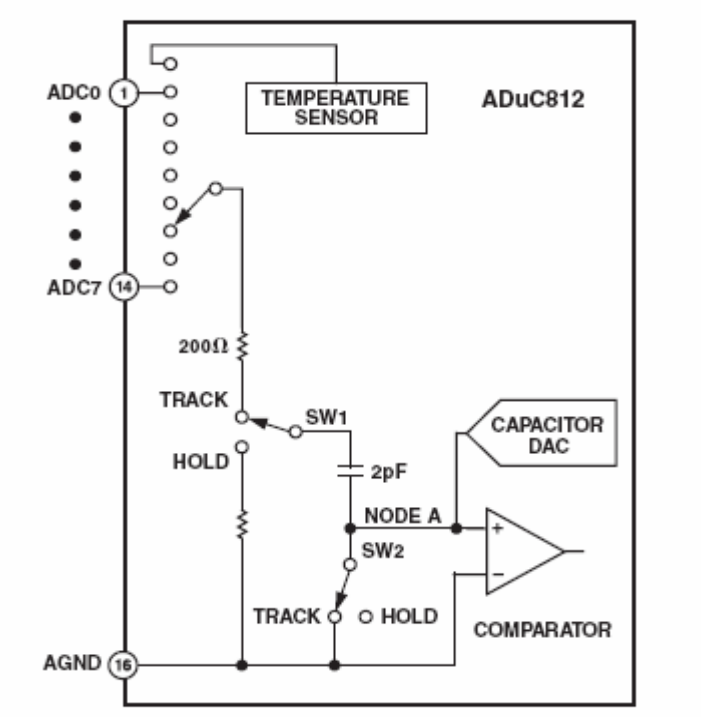

Fig. A.1 Internal ADC structure [22].

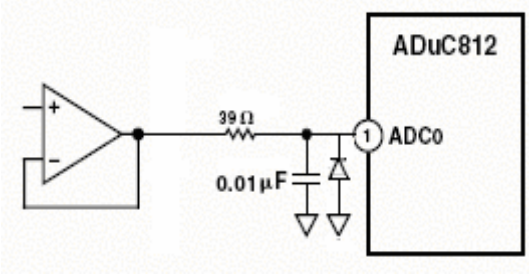

Fig. A.2 Buffering of the analog inputs.

DC leakage currents at the ADuC812's analog inputs causes measurable dc errors with external source impedances of as little as 100 Ω, thus a larger capacitor can be used if desired, but not a larger resistor. To ensure accurate ADC operation, the total source impedance at each analog input is kept less than 61 Ω [22]. We have used the lower diode to ensure that the analog input is protected from the under voltage condition.

Appendix B

POWER REQUIREMENT

Pulse Oximeter

Power supply	-	±5 V DC regulated power supply.
Current	-	60 mA from +5 V and 40mA from –5 V.

APPENDIX C

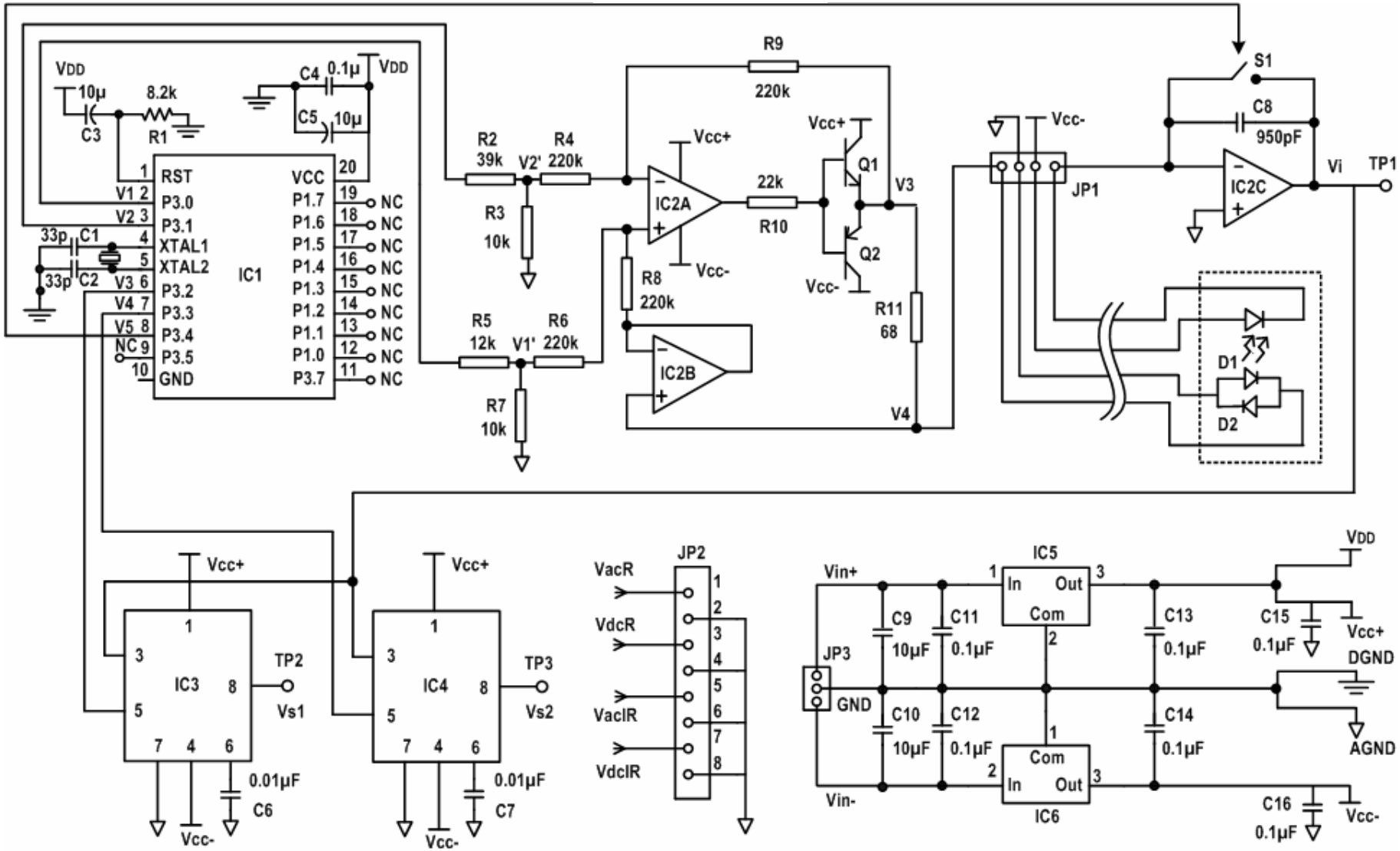

Fig. C.1 Timing and control (TAC) circuit: Power supply and signal conditioning block.

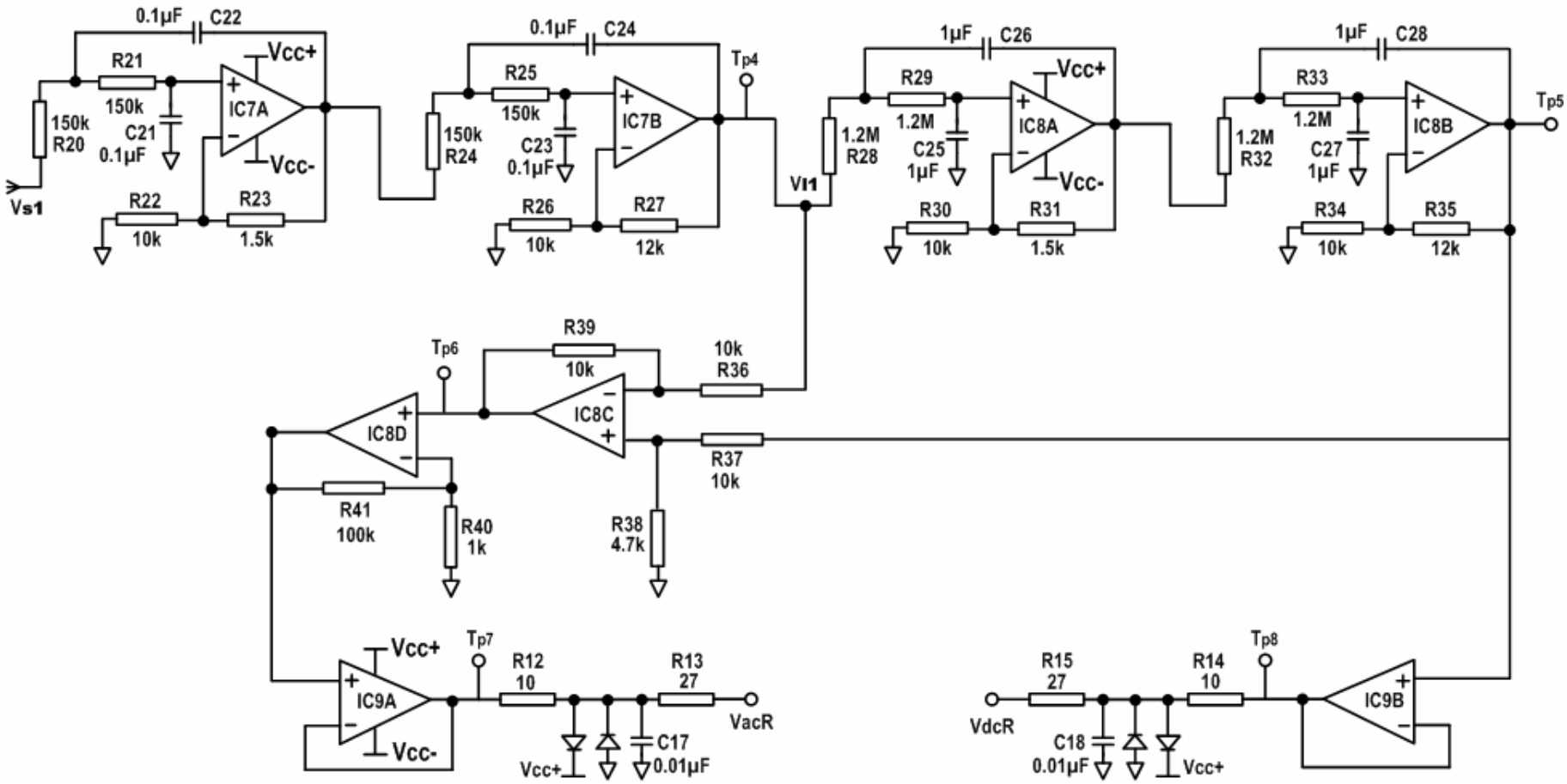

Fig. C.2 Analog filter for red plethysmogram signal.

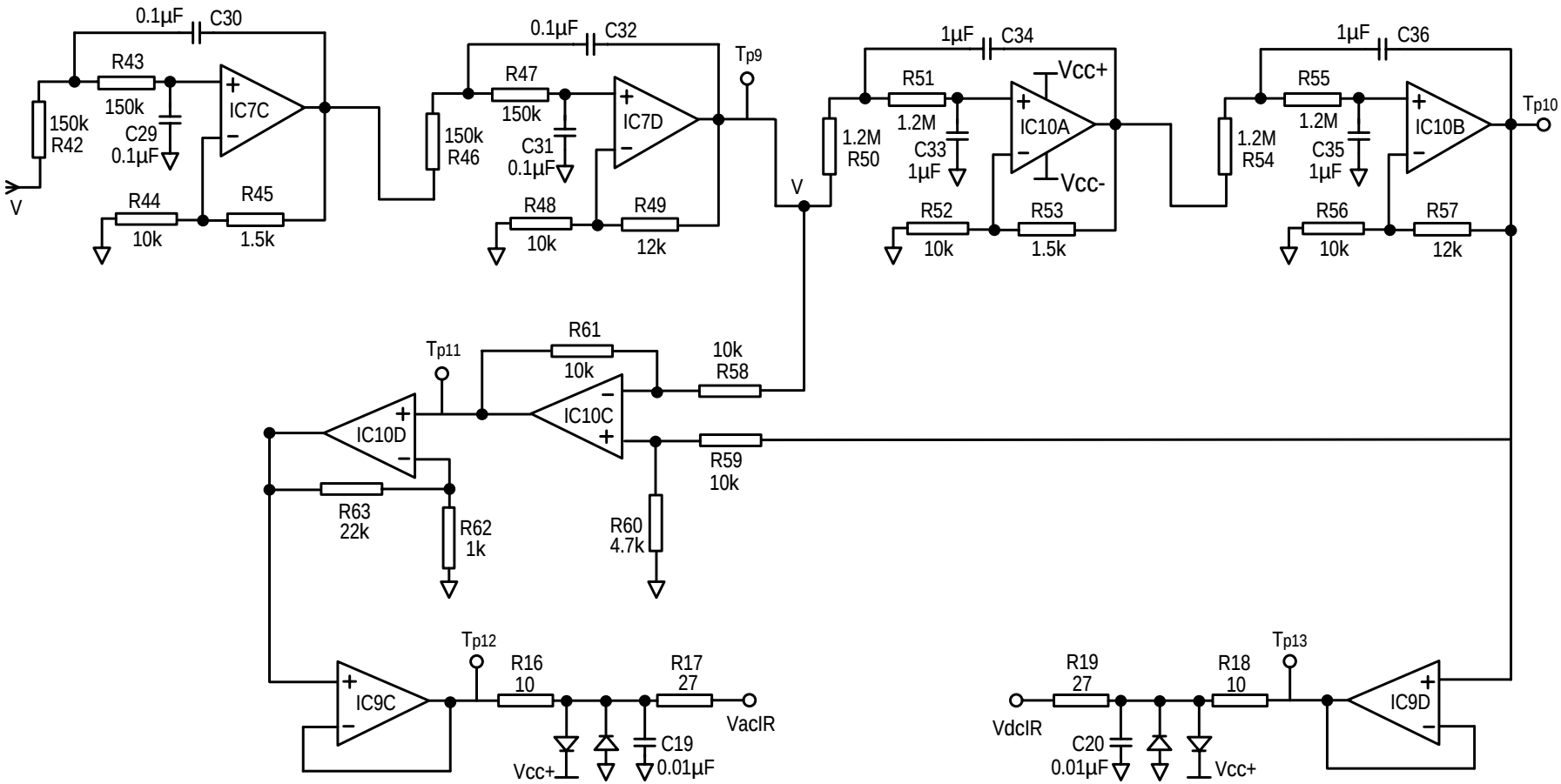

Fig. C.3 Analog filter for infrared plethysmogram signal.

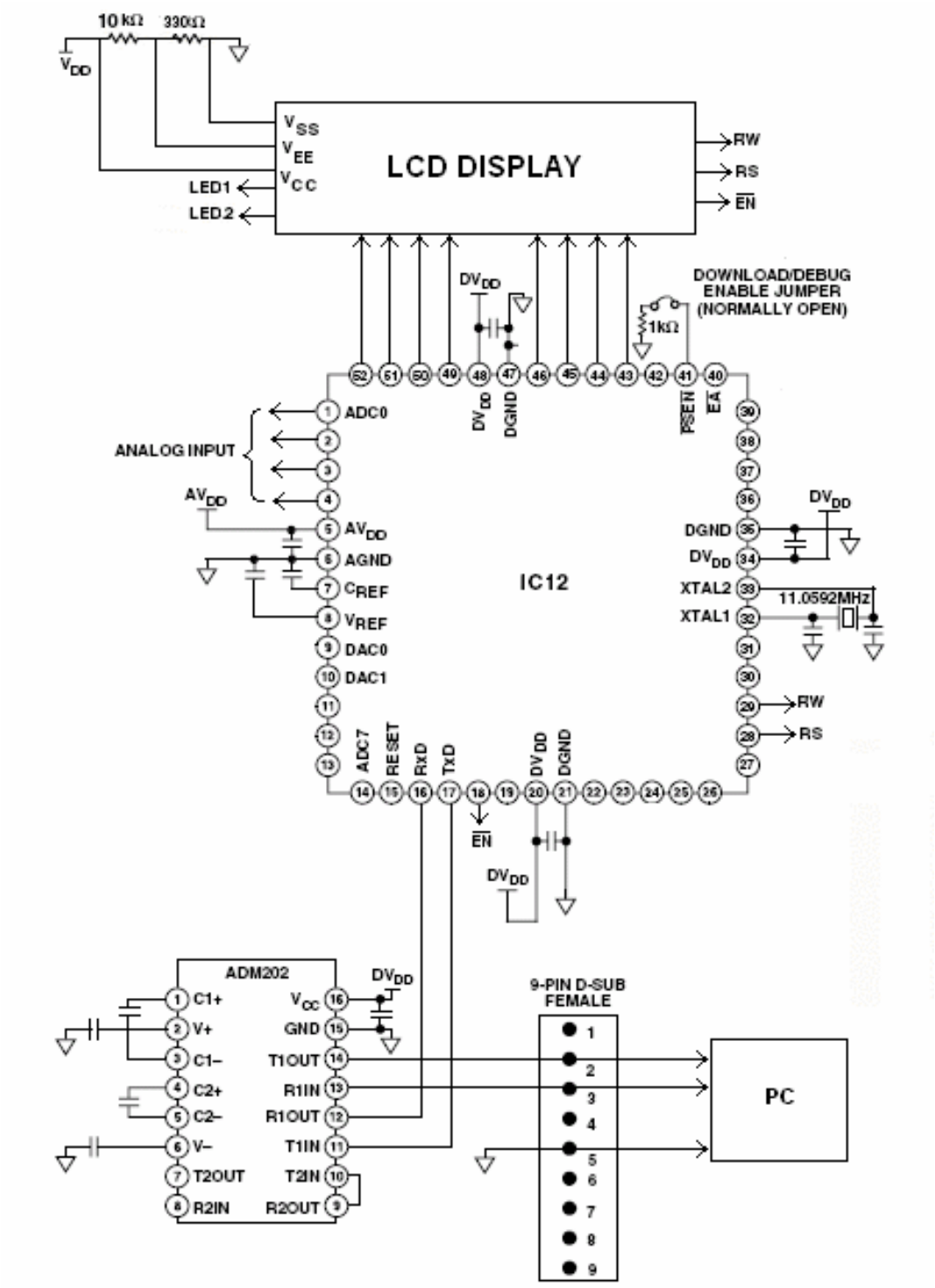

Fig. C.4 Acquisition, processing and display (APD) circuit.

REFERENCES

[1] M. Yitzhak and B. D. Ochs, "Noninvasive pulse oximetry utilizing reflectance photoplethysmography," *IEEE Trans. Biomed. Eng*, vol. 35, pp. 798–805, Oct. 1988.

[2] V. Kamat, "Pulse oximetry," *Indian J. Anaesth.*, vol. 46(4): pp. 261–268, 2002.

[3] P. D. Mannheimer, J. R. Casciani, M. E. Fein, and S. L. Nierlich, "Wavelength selection for low-saturation pulse oximetry," *IEEE Trans. Biomed. Eng*, vol. 44, pp. 148–158, Mar. 1997.

[4] M. J. Hayes and P. R. Smith, "A new method for pulse oximetry possessing inherent insensitivity to artifact," *IEEE Trans. Biomed. Eng*, vol. 48, pp. 452–460, Apr. 2001.

[5] S. S. Adsul, "Pulse oximeter," M.Tech. Dissertation, Supervisor: R. Lal, School of Biomedical Engineering, IIT Bombay, 2001.

[6] M. Ingle, "Finger tip pulse oximeter," M.Tech. Dissertation, Supervisor: R. Lal, School of Biomedical Engineering, IIT Bombay, 1996.

[7] P. A. Kyriacou, S. Powell, R. M. Langford, and D. P. Jones, "Esophageal pulse oximetry utilizing reflectance photo plethysmography," *IEEE Trans. Biomed. Eng*, vol. 49, pp. 1360–1368, Nov. 2002.

[8] J. Lee, W. Jung, I.T. Kang, Y. Kim, and G. Lee, "Design of filter to reject motion artifact of pulse oximetry," *Computer Standards & Interfaces*, vol. 26, pp. 241–249, 2004.

[9] "Principles of pulse oximeter," http://www.oximeter.org/pulseox/principles.htm, Sep 2002, downloaded on 22nd Apr. 2005.

[10] J. Bachiochi, "Light-to-frequency conversion (part 1)," *Circuit Cellar*, issue 173, pp. 26–31, Dec. 2004.

[11] H. Asada, P. Shaltis, and S. Rhee, "Validation and benchmarking of a high-speed modulation design for oxygen saturation measurement using photo plethysmographic ring sensors," Final Report No. 3-4, HAHC, d' Arbeloff Laboratory for information systems and Technology, MIT, Sep 2002.

[12] J. M. Schmitt, "Simple photon diffusion analysis of the effects of multiple scattering on pulse oximetry," *IEEE Trans. Biomed Eng*, vol. 38, pp. 1194–1203, Dec. 1991.

[13] A. Zourabian, A. Siegel, B. Chance, N. Ramanujan, M. Rode, and D. A. Boas, "Trans-abdominal monitoring of fetal arterial blood oxygenation using pulse oximetry," *Journal of Biomedical Optics*, vol. 5(4), pp. 391–405, Oct. 2000.

[14] Y. Pole "Evolution of pulse oximeter," *International Congress Series*, pp. 137–138, 2002.

[15] "NPB-290 Service manual," http://www.mallinckrodt.com/respiratory/resp/Serv_Supp/PDFs/550/067857A_SRV_N550.pdf, Nellcor Puritan Bennett Inc., Pleasanton, CA, USA, downloaded on Mar. 2005.

[16] "504DX series service manual," Criticare systems Inc., Waukesha, WI, USA, Jan. 1999.

[17] "Pulse oximeters," http://www.smiths-bci.com/HTML/Products/pulse_oximeters.htm, site of Smiths Medical PM, Inc., Waukesha, WI, USA, downloaded on May 2005.

[18] "Oximetry," http://www.gehealthcare.com/usen/oximetry/products/3900p_pulse.html, site of G E Healthcare, Chalfont St. Giles, UK, downloaded on May 2005.

[19] "Rad-9 standalone pulse Oximeter," http://www.masimo.com/pulseox/rad9.htm, Irvine, WI, USA, downloaded on Jun. 2005

[20] J. Bachiochi, "Light-to-frequency conversion (part 2)," *Circuit Cellar*, issue 174, pp. 68–71, Jan. 2005.

[21] "Photo diode," http://www.tpub.com/neets/book7/26g.htm, downloaded on 7th Mar. 2005.

[22] **"**ADuC812 data sheets,**"** http://www.analog.com/UploadedFiles/Data_Sheets/11291590 ADuC812_e.pdf, downloaded on Mar. 2005.

[23] P. K. Lehana and P. C. Pandey, "A low cos impedance glottograph and pitch analyzer," *Proc. Bio Vision 2001InternationalConference on Biomedical Engineering*, (Bangalore, India), pp**.** 33–37, Dec. 2001.

[24] J. M. Fiore, *Op Amps and Linear Iintegrated Circuits*, Albany, New York: Delmar, 2001.

[25] F. R. Dungan, *Op Amps & Linear Integrated Circuits for Technicians*, 2nd ed. Albany, New York: Delmar, 1992.

[26] K. R. Botkar, *Integrated Circuits*, 7th ed., Delhi: Khanna Publishers, 1989.

[27] S. Rhee, B-H. Yang, and H. H. Asada, "Artifact-resistant power-efficient design of finger-ring plethysmographic sensor," *IEEE Trans. on Biomed Eng*, vol. 48, pp. 795–805, July 2001.